Check for updates

Received: 22 March 2023 | Accepted: 17 July 2023

DOI: 10.1111/arcm.12906

ORIGINAL ARTICLE

Reflections into Ptolemaic Glass II: Characterizing Yellow, Yellowish-orange, Red, and Brown Inlays from Tebtynis

Cinzia Bettineschi[1,2] | **Ivana Angelini**[2]

[1]Department of Classical Archaeology, University of Augsburg, Augsburg, Germany

[2]Department of Cultural Heritage: Archaeology and History of Art, Cinema and Music, Università degli Studi di Padova, Padua, Italy

Correspondence
Cinzia Bettineschi, Department of Classical Archaeology, University of Augsburg, Universitätsstraße 10, Augsburg 86159, Germany.
Email: cinzia.bettineschi@philhist.uni-augsburg.de

Funding information
Analyses were funded by the University of Padova among the most innovative research proposed by students (proposing PhD student: CB; reference professor: IA) in the framework of project "ArExGlass: Archaeometry and Experimental Archaeology for pre-Roman Glassworking" (2017–2018).

Abstract

A systematic and extensive analytical study was carried out on the loose inlays discovered in the Ptolemaic workshop of Tebtynis (Fayum oasis, Egypt). This paper presents data derived from the multi-methodological archaeometric investigations (optical microscopy, scanning electron microscopy–energy-dispersive spectroscopy, electron probe microanalysis, micro-Raman spectroscopy) performed on a set of intentionally colored and opacified glasses. In particular, we will discuss the textural, chemical, and mineralogical results related to the study of the yellow, yellowish-orange, red, and brown inlays and semi-finished/waste products now preserved at the Museo Egizio, Torino. The results highlight the presence of natron (low-magnesium glasses, LMG) and plant ash (high-magnesium glasses, HMG) base glass, coexisting with intermediate composition. Yellow samples are opacified using lead antimonates doped with iron and sometimes tin; conversely, yellowish-orange specimens and the only brown sample are characterized by nanocrystals of cuprite. Red glasses are found in two variants: Dull reds are HMG with colloidal metallic copper particles, while sealing-wax reds show LMG composition, associated with dendritic cuprite dispersed in a transparent, greenish matrix.

KEYWORDS

colorants, opacifiers, polychrome inlays, Ptolemaic glass, secondary workshop

This is an open access article under the terms of the Creative Commons Attribution-NonCommercial-NoDerivs License, which permits use and distribution in any medium, provided the original work is properly cited, the use is non-commercial and no modifications or adaptations are made.

© 2023 The Authors. *Archaeometry* published by John Wiley & Sons Ltd on behalf of University of Oxford.

INTRODUCTION

The Ptolemaic period stands as a watershed in the technological evolution of vitreous materials, as it set the basis for the transformation of glass from a luxury product to a mass-produced commodity following the introduction and spread of glassblowing (Grose, 1989; Stern, 2012). It is thus natural to wonder if the birth of glassblowing can be associated with eventual changes in the composition or technology of glass during the late 4th to 1st century BCE. However, despite the key role of this phase, only the main points of Ptolemaic recipes have been investigated to date, and the glass of this period is usually regarded as a predecessor of its Roman counterpart, without specific chemical or technological markers. Although there are some positive exceptions (e.g., Bimson & Freestone, 1988; Brill, 1999; Nenna & Gratuze, 2009), Ptolemaic glass is generally under-investigated by recent archaeometric works. This, of course, is also due to the problems in accessing and sampling the objects themselves. The major concerns, when reading the specialized literature, are regarded as the recurrent absence of an accurate chronological or geographic framework for the archaeological materials, the low number of analyzed specimens in each dataset, and the lack of archaeometric data on glasses from actual craft areas.

The study of the colored inlays unearthed in the secondary workshop of Tebtynis offers an exceptional window into the complexity of the glass-coloring/opacifying technologies employed by the ancient Egyptian artisans during the Ptolemaic period. In this paper, we will present the results of a multi-analytical investigation on 59 samples of opaque yellow, yellowish-orange, red, and brown glasses selected among the inlays from Tebtynis preserved at the Museo Egizio, Torino. The aim is to contribute to developing a reference database on the distinctive compositional and technological traits of Ptolemaic glasses to shed new light on this crucial moment in the history of glass.

MATERIALS AND METHODS

The Tebtynis collection of the Museo Egizio comprises more than 800 elements in monochrome, stratified, and mosaic glass. Most of these objects can be interpreted as finished inlays, but there are also a significant number of semi-finished and waste products. Of the eight main color classes identified in the set, the yellow, yellowish-orange, red (both sealing-wax and dull red), and opaque brown glasses comprise 59 analyzed specimens (Supporting Information Table S1, which includes images of each object). Opaque brown glass is represented only by a single occurrence in the bichrome bar S-MR-502; similarly, yellow glass was never found on its own but only in polychrome combinations. Red glasses (dull red and sealing-wax red), on the contrary, are commonly used for figured inlays (sometimes with surface gold foils) and for numerous types of monochrome bars, stratified glasses, and mosaic compositions. Yellowish-orange glasses were never seen in figurative inlays but are frequently found as monochrome bars and in polychrome pieces.

The analytic protocol used to characterize the samples conforms to the one employed for the study of the transparent, white, blue, and green glasses from the same set. Thus, the reader is referred to Bettineschi and Angelini (2022) for details regarding the experimental conditions. The supplementary materials accompanying that paper also include the measured electron probe microanalysis (EPMA) data of Corning standards A and B, along with the corresponding errors compared to the certified values. Those data are also applicable to the set of materials presented in this study as they were analyzed in the same sessions.

After a first screening of the inlays by stereoscopic microscopy (SM), the objects were sampled, mounted in epoxy resin, polished, and coated with carbon film. The following complementary techniques were used for the textural, chemical, and mineralogical investigation of the samples (Supporting Information Table S2): optical microscopy (OM) for preliminary textural

14754754, 2024, 1, Downloaded from https://onlinelibrary.wiley.com/doi/10.1111/arcm.12906 by CochraneItalia, Wiley Online Library on [04/02/2025]. See the Terms and Conditions (https://onlinelibrary.wiley.com/terms-and-conditions) on Wiley Online Library for rules of use; OA articles are governed by the applicable Creative Commons License

observations; scanning electron microscopy coupled with energy-dispersive spectroscopy (SEM-EDS), for high-resolution morphological and chemical imaging, and qualitative chemical data; EPMA to determine the chemistry of the amorphous phase; and micro-Raman for identification of the crystalline inclusions (relics of the batch, colorants/opacifiers, and newly formed phases). Given the wide variability in the composition of the glassy matrix and of the coloring/opacifying agents, the results will be presented and discussed separately for each of the main groups identified: yellow glasses; dull red glasses; and brown, yellowish-orange, and sealing-wax red glasses. The composition of the base glass can be calculated and is referred to in the paper as a reduced composition (Supporting Information Table S3).

RESULTS

Yellow glasses

According to the EPMA data (Table 1), the alkali composition of yellow samples shows magnesia ranging from 0.35% to 1.01%, potash from 0.49% to 0.96%, and soda of the order of 11.82–15.04%, except in a few weathered samples (Figure 1a). The overall base glass composition is well consistent with the classic low-magnesium, "natron" glasses (LMG). Moreover, PbO ranges from 5.34% to 16.04%, and Sb_2O_5 reaches values of 0.86–4.15% (Figure 1b).

The opacity and color of the yellow glasses are due to the presence of small, anhedral inclusions of lead and lead–tin antimonates, as demonstrated by SEM-EDS (Figure 2), wavelength-dispersive X-ray spectroscopy (WDS), and micro-Raman data (Figure 3a; the composition is discussed in the text below). The dimensions of the aggregates vary widely from 20 μm to submicrometric size. Textural examinations also show that many yellow glasses are characterized by diffuse chemical zonings with alternating stripes richer and poorer in lead, the latest bearing the highest concentration of antimonate crystallites (Figure 2a).

However, three of the eight yellow samples show a homogeneous texture. In addition to lead antimonates, P-A-402-G also includes numerous, rounded quartz grains with unreacted edges (micro-Raman data), reaching up to 50 μm (Figure 2c,d). Considering their very high number and rather homogeneous distribution, they can most probably be interpreted as intentional additives, rather than unintentional relics of the sand in the original batch.

P-FL-501-G revealed the presence of abundant, euhedral calcium antimonate crystals ($CaSb_2O_6$), together with lead–tin antimonates as determined by a combination of micro-Raman and WDS data (Figure 2b). The presence of hexagonal calcium antimonates might have been voluntary, in order to obtain a clearer yellow, but is more probably related to the conversion from lead to calcium antimonates that takes place during firing at more than 1000°C, as demonstrated by the experimental replicas of Molina et al. (2014). Other inclusions in this sample comprise one small crystal of iron oxide, possibly a relic of the sand used, and one newly formed cluster of pyroxene crystals.

It is interesting to observe that yellow glasses with different textures can be present even within the same inlay. For examples, FR-422-G1 is characterized by the absence of a banded texture, in contrast to FR-422-G2, which was used for other parts of the same inlay (Figure 2e).

SEM–backscattered electron (BSE) observations showed in FR-422-G1 a very high number of Pb-Ca-Na silicates, with different stoichiometric ratios (EDS data), sometimes growing in larger, radial aggregates reaching up to 40–50 μm. Their composition is consistent with the combination of the main constituents of the vitreous phase and can be interpreted in terms of devitrification products. The sample also shows a couple of quartz crystals, which are rather common in yellow glasses, often as residues from the sand (Figure 2f).

Considering the WDS composition of the nine analyzed antimonates in yellow glasses, it is possible to distinguish two main pigment types: lead antimonates (three occurrences), with PbO

14754754, 2024, 1, Downloaded from https://onlinelibrary.wiley.com/doi/10.1111/arcm.12906 by CochraneItalia, Wiley Online Library on [04/02/2025]. See the Terms and Conditions (https://onlinelibrary.wiley.com/terms-and-conditions) on Wiley Online Library for rules of use; OA articles are governed by the applicable Creative Commons License

TABLE 1 Electron probe microanalysis (EPMA) results. Chemical composition of the amorphous phase in the analyzed samples (EPMA data expressed as oxide weight percent), as a mean of 5- to 7-point analyses.

Sample name	Glass color		Na_2O	MgO	Al_2O_3	SiO_2	SO_3	P_2O_5	Cl	K_2O	CaO	TiO_2	MnO	FeO	CoO	CuO	As_2O_5	SnO_2	Sb_2O_5	PbO	Total
I-RAu-605	Sealing-wax red	Mean	11.51	0.47	1.99	46.17	0.05	0.48	0.54	0.46	4.19	0.12	0.15	0.72	0.01	4.19	0.03	0.31	1.44	26.93	99.76
		SD	0.12	0.04	0.09	0.23	0.02	0.06	0.02	0.01	0.02	0.04	0.02	0.08	0.02	0.16	0.05	0.01	0.02	0.28	
I-RAu-622	Sealing-wax red	Mean	11.92	0.61	1.64	53.51	0.33	0.08	0.62	0.65	5.93	0.09	0.14	0.89	0.01	4.31	0.02	0.10	0.41	16.67	97.95
		SD	0.10	0.03	0.01	0.41	0.08	0.04	0.03	0.02	0.06	0.02	0.04	0.08	0.02	0.25	0.01	0.03	0.08	0.10	
M-Ar-506	Yellowish-orange	Mean	8.41	0.37	1.58	46.84	0.14	0.42	0.41	0.62	4.70	0.07	0.06	1.25	0.00	9.36	0.03	0.02	1.90	25.01	101.18
		SD	0.20	0.05	0.04	0.13	0.04	0.04	0.05	0.01	0.04	0.05	0.03	0.06	0.00	0.43	0.02	0.01	0.09	0.58	
M-Ar-506a	Yellowish-orange	Mean	10.70	1.91	3.04	45.37	0.17	0.70	0.59	1.28	8.01	0.31	0.24	1.91	0.02	7.23	0.03	0.63	0.33	16.06	98.56
		SD	0.26	0.04	0.07	0.29	0.05	0.04	0.05	0.02	0.05	0.02	0.04	0.11	0.03	0.25	0.03	0.02	0.04	0.25	
M-G-504	Yellowish-orange	Mean	6.69	0.29	1.53	42.15	0.26	0.12	0.31	0.50	1.96	0.15	0.08	1.79	0.05	6.91	0.02	0.02	2.52	30.92	96.29
		SD	0.23	0.02	0.06	0.49	0.07	0.05	0.15	0.02	0.07	0.02	0.04	0.17	0.04	0.79	0.03	0.02	0.17	0.70	
M-G-504a	Yellowish-orange	Mean	11.02	1.61	2.74	45.15	0.67	0.39	0.71	1.06	6.93	0.25	0.20	2.20	0.02	8.03	0.03	0.94	0.45	18.18	100.58
		SD	0.16	0.04	0.03	0.35	0.03	0.07	0.03	0.03	0.08	0.02	0.04	0.05	0.02	0.27	0.03	0.05	0.04	0.50	
M-G-504b	Yellowish-orange	Mean	10.95	1.56	2.73	44.02	0.67	0.35	0.68	1.05	6.86	0.23	0.26	2.15	0.02	8.21	0.05	0.95	0.42	17.80	98.96
		SD	0.13	0.04	0.06	0.52	0.07	0.08	0.03	0.02	0.06	0.07	0.02	0.08	0.03	0.23	0.03	0.03	0.04	0.51	
M-R-501	Dull red	Mean	13.76	2.29	2.12	55.10	0.82	0.34	0.92	1.58	8.36	0.17	0.31	1.32	0.02	2.27	0.02	0.44	0.37	8.43	98.61
		SD	0.24	0.09	0.08	1.25	0.04	0.16	0.04	0.03	0.40	0.03	0.05	0.08	0.02	0.19	0.02	0.04	0.06	0.43	
M-R-502d	Sealing-wax red	Mean	10.47	0.84	2.85	41.29	0.05	0.29	0.52	0.50	1.49	0.52	0.23	1.54	0.05	4.11	0.03	0.00	0.00	35.08	99.85
		SD	0.26	0.02	0.05	0.44	0.01	0.05	0.01	0.02	0.02	0.06	0.05	0.04	0.06	0.09	0.02	0.00	0.00	0.80	
M-R-505	Dull red	Mean	14.01	2.29	2.26	56.29	0.27	0.76	0.94	1.60	8.55	0.19	0.07	1.02	0.01	1.69	0.03	0.41	0.36	7.96	98.72
		SD	0.16	0.03	0.05	0.35	0.02	0.04	0.06	0.02	0.12	0.03	0.02	0.04	0.02	0.07	0.02	0.06	0.01	0.08	
M-R-507	Sealing-wax red	Mean	11.78	0.60	1.69	53.99	0.13	0.35	0.68	0.64	5.69	0.07	0.48	1.13	0.03	5.85	0.03	0.10	0.40	16.51	100.13
		SD	0.13	0.02	0.03	0.40	0.01	0.03	0.03	0.03	0.11	0.03	0.02	0.07	0.02	0.12	0.03	0.03	0.05	0.71	
M-RAu-502	Sealing-wax red	Mean	10.06	0.84	1.87	38.87	0.24	0.34	0.73	0.63	4.65	0.15	0.13	1.18	0.02	4.04	0.00	1.12	0.51	34.25	99.63
		SD	0.06	0.03	0.11	0.51	0.02	0.03	0.01	0.01	0.07	0.01	0.05	0.05	0.03	0.11	0.00	0.02	0.04	0.47	

14754754, 2024, 1, Downloaded from https://onlinelibrary.wiley.com/doi/10.1111/arcm.12906 by CochraneItalia, Wiley Online Library on [04/02/2025]. See the Terms and Conditions (https://onlinelibrary.wiley.com/terms-and-conditions) on Wiley Online Library for rules of use; OA articles are governed by the applicable Creative Commons License

TABLE 1 (Continued)

Sample name	Glass color		Na_2O	MgO	Al_2O_3	SiO_2	SO_3	P_2O_5	Cl	K_2O	CaO	TiO_2	MnO	FeO	CoO	CuO	As_2O_5	SnO_2	Sb_2O_5	PbO	Total
M-RAu-502a	Sealing-wax red	Mean	11.80	0.61	1.73	54.12	0.08	0.40	0.64	0.65	5.74	0.13	0.55	1.06	0.03	5.61	0.00	0.11	0.41	16.92	100.59
		SD	0.15	0.04	0.05	0.19	0.05	0.11	0.01	0.01	0.01	0.07	0.08	0.11	0.02	0.15	0.01	0.01	0.06	0.04	
M-RAu-502b	Sealing-wax red	Mean	11.57	0.47	1.48	54.22	0.40	0.09	0.69	0.66	4.21	0.08	0.43	0.46	0.01	4.47	0.01	0.11	1.61	15.50	96.53
		SD	0.11	0.03	0.03	0.36	0.02	0.02	0.02	0.03	0.05	0.02	0.12	0.08	0.02	0.39	0.02	0.02	0.07	0.52	
M-RAu-502c	Sealing-wax red	Mean	10.39	0.54	2.02	54.21	0.11	0.25	0.58	0.79	5.49	0.11	0.62	1.00	0.01	6.18	0.00	0.00	0.41	17.84	100.55
		SD	0.05	0.03	0.05	0.07	0.02	0.07	0.03	0.02	0.04	0.06	0.04	0.04	0.01	0.08	0.00	0.00	0.02	0.31	
P-A-402-G	Yellow	Mean	5.93	0.21	1.14	46.90	0.20	0.07	0.38	0.34	3.01	0.07	0.03	1.10	0.02	0.06	0.00	0.00	1.48	36.53	97.52
		SD	0.10	0.04	0.03	0.63	0.01	0.02	0.04	0.02	0.13	0.02	0.03	0.34	0.03	0.02	0.00	0.00	0.20	0.91	
P-A-408-Ar	Yellowish-orange	Mean	11.20	1.53	2.59	45.56	0.30	0.62	0.57	1.05	7.09	0.27	0.31	2.13	0.10	6.89	0.03	0.85	0.43	17.60	99.15
		SD	0.32	0.08	0.12	0.61	0.01	0.05	0.02	0.05	0.13	0.03	0.00	0.02	0.05	0.18	0.06	0.03	0.02	0.52	
P-A-418-R1	Dull red	Mean	13.59	2.85	2.48	56.47	1.36	0.17	1.05	1.90	7.96	0.17	0.54	1.67	0.01	2.02	0.01	0.44	0.41	7.66	100.76
		SD	0.27	0.02	0.06	0.48	0.03	0.04	0.03	0.02	0.07	0.01	0.05	0.09	0.02	0.19	0.01	0.03	0.05	0.31	
P-A-418-R2	Dull red	Mean	13.81	2.92	2.53	55.79	1.32	0.19	1.04	2.02	7.89	0.18	0.52	1.63	0.03	1.86	0.01	0.45	0.42	7.79	100.40
		SD	0.14	0.06	0.10	0.24	0.03	0.05	0.03	0.01	0.04	0.04	0.05	0.05	0.03	0.11	0.02	0.03	0.03	0.22	
P-A-419-R	Dull red	Mean	12.42	3.38	1.89	60.55	1.60	0.16	0.82	3.00	7.42	0.12	0.62	2.70	0.03	1.46	0.13	0.72	0.27	3.67	100.97
		SD	0.16	0.03	0.04	0.18	0.08	0.02	0.02	0.04	0.04	0.07	0.03	0.02	0.05	0.08	0.04	0.03	0.04	0.10	
P-CR-421-G1	Yellow	Mean	12.62	1.01	1.86	63.61	0.25	0.25	0.90	0.58	4.69	0.09	0.47	1.81	0.01	0.06	0.05	0.12	1.09	11.91	101.37
		SD	0.39	0.37	0.07	1.33	0.12	0.04	0.03	0.10	0.22	0.02	0.16	0.27	0.02	0.05	0.05	0.05	0.15	1.17	
P-CR-421-G2	Yellow	Mean	10.79	0.40	1.84	53.93	0.06	0.14	0.59	0.57	2.20	0.12	0.42	2.67	0.00	0.16	0.02	0.04	1.35	23.10	98.38
		SD	0.63	0.08	0.11	4.05	0.05	0.05	0.07	0.21	0.42	0.02	0.04	0.37	0.00	0.16	0.02	0.02	0.29	5.71	
P-CR-421-R	Dull red	Mean	13.89	2.77	2.45	56.77	1.09	0.24	0.99	1.95	8.24	0.17	0.45	1.45	0.01	1.66	0.04	0.42	0.34	7.38	100.29
		SD	0.22	0.08	0.03	0.24	0.06	0.04	0.02	0.09	0.07	0.04	0.03	0.05	0.02	0.22	0.03	0.04	0.05	0.24	
P-FL-004-R	Dull red	Mean	14.72	2.37	2.29	57.19	0.84	0.22	0.94	1.49	8.50	0.20	0.32	1.30	0.00	2.03	0.00	0.46	0.33	8.40	101.61
		SD	0.19	0.02	0.02	0.36	0.05	0.08	0.06	0.09	0.09	0.05	0.02	0.04	0.01	0.19	0.00	0.04	0.04	0.15	

(Continues)

14754754, 2024, 1, Downloaded from https://onlinelibrary.wiley.com/doi/10.1111/arcm.12906 by CochraneItalia, Wiley Online Library on [04/02/2025]. See the Terms and Conditions (https://onlinelibrary.wiley.com/terms-and-conditions) on Wiley Online Library for rules of use; OA articles are governed by the applicable Creative Commons License

TABLE 1 (Continued)

Sample name	Glass color		Na_2O	MgO	Al_2O_3	SiO_2	SO_3	P_2O_5	Cl	K_2O	CaO	TiO_2	MnO	FeO	CoO	CuO	As_2O_5	SnO_2	Sb_2O_5	PbO	Total
P-FL-501-G	Yellow	Mean	13.00	0.77	2.14	64.79	0.22	0.38	0.69	0.96	3.52	0.13	0.27	1.26	0.02	0.13	0.01	0.14	4.15	7.12	99.68
		SD	0.28	0.02	0.07	1.13	0.02	0.00	0.05	0.04	0.06	0.03	0.03	0.03	0.03	0.11	0.02	0.03	0.09	0.21	
P-FL-501-R	Dull red	Mean	12.54	2.37	2.73	53.81	1.05	0.26	0.84	1.39	9.13	0.30	0.39	1.90	0.01	2.15	0.01	0.52	0.25	10.00	99.65
		SD	0.08	0.03	0.05	0.51	0.04	0.06	0.03	0.06	0.09	0.04	0.05	0.03	0.03	0.37	0.03	0.04	0.02	0.17	
P-FR-422-G1	Yellow	Mean	15.04	0.53	2.16	65.90	0.09	0.23	1.14	0.56	5.58	0.10	0.13	1.35	0.01	0.03	0.00	0.01	0.93	6.56	100.35
		SD	0.15	0.06	0.04	0.96	0.03	0.04	0.12	0.06	0.34	0.01	0.04	0.63	0.02	0.02	0.00	0.02	0.05	0.57	
P-FR-422-G2	Yellow	Mean	12.96	0.59	2.11	58.33	0.09	0.21	0.98	0.60	3.88	0.13	0.53	1.78	0.00	0.05	0.03	0.05	0.86	16.04	99.21
		SD	0.14	0.05	0.02	0.34	0.03	0.06	0.05	0.07	0.13	0.02	0.01	0.10	0.00	0.03	0.04	0.02	0.10	0.32	
P-FR-422-R	Dull red	Mean	14.90	2.37	2.34	56.76	0.81	0.24	1.00	1.48	8.43	0.18	0.35	1.29	0.02	1.76	0.01	0.43	0.33	8.28	100.98
		SD	0.08	0.05	0.05	0.45	0.05	0.02	0.02	0.03	0.09	0.04	0.04	0.05	0.02	0.23	0.01	0.06	0.04	0.15	
P-R-414-G	Yellow	Mean	13.64	0.39	1.87	62.36	0.03	0.20	1.11	0.52	4.12	0.09	0.15	1.33	0.03	0.05	0.01	0.05	1.07	12.44	99.45
		SD	0.28	0.03	0.04	0.46	0.03	0.02	0.08	0.00	0.12	0.09	0.04	0.20	0.02	0.02	0.02	0.02	0.14	0.12	
P-R-419-Ar	Yellowish-orange	Mean	10.79	1.76	2.93	44.14	0.66	0.23	0.46	1.09	7.36	0.24	0.24	1.83	0.03	6.31	0.03	0.80	0.48	19.33	98.70
		SD	0.19	0.04	0.04	0.37	0.06	0.02	0.03	0.04	0.11	0.04	0.03	0.05	0.04	0.46	0.04	0.07	0.03	0.51	
P-R-419-G	Yellow	Mean	1.07	0.37	1.74	65.82	0.03	0.19	1.36	0.74	4.04	0.09	0.18	1.33	0.01	0.03	0.01	0.04	1.11	12.88	91.03
		SD	1.29	0.04	0.07	0.53	0.03	0.03	0.06	0.18	0.19	0.03	0.02	0.15	0.02	0.02	0.01	0.02	0.23	0.62	
P-R-419-R	Sealing-wax red	Mean	11.27	1.84	2.99	44.27	0.64	0.24	0.48	1.06	7.18	0.24	0.23	1.87	0.00	6.19	0.05	0.80	0.50	19.93	99.78
		SD	0.38	0.02	0.06	0.42	0.07	0.04	0.01	0.02	0.05	0.04	0.05	0.16	0.00	1.40	0.05	0.05	0.04	0.81	
P-R-423-Ar	Yellowish-orange	Mean	11.55	1.61	2.80	45.93	0.67	0.58	0.71	1.10	7.02	0.25	0.28	2.26	0.00	6.87	0.02	0.91	0.46	16.67	99.68
		SD	0.15	0.03	0.03	0.42	0.04	0.17	0.02	0.02	0.07	0.03	0.04	0.01	0.00	0.74	0.04	0.06	0.06	0.65	
P-R-423-G	Yellow	Mean	13.12	0.35	1.76	64.60	0.05	0.25	1.26	0.52	4.13	0.07	0.15	1.21	0.00	0.08	0.02	0.06	1.05	11.59	100.25
		SD	0.24	0.03	0.08	0.63	0.03	0.11	0.10	0.01	0.10	0.02	0.03	0.23	0.00	0.06	0.01	0.03	0.12	0.29	
P-R-423-R1	Sealing-wax red	Mean	12.41	1.60	2.85	46.93	0.64	0.43	0.68	1.23	7.25	0.31	0.27	2.46	0.01	5.09	0.06	0.93	0.46	17.05	100.65
		SD	0.30	0.07	0.05	0.33	0.06	0.07	0.04	0.02	0.07	0.06	0.08	0.03	0.02	0.14	0.06	0.02	0.05	0.41	

14754754, 2024, 1, Downloaded from https://onlinelibrary.wiley.com/doi/10.1111/arcm.12906 by CochraneItalia, Wiley Online Library on [04/02/2025]. See the Terms and Conditions (https://onlinelibrary.wiley.com/terms-and-conditions) on Wiley Online Library for rules of use; OA articles are governed by the applicable Creative Commons License

TABLE 1 (Continued)

Sample name	Glass color		Na_2O	MgO	Al_2O_3	SiO_2	SO_3	P_2O_5	Cl	K_2O	CaO	TiO_2	MnO	FeO	CoO	CuO	As_2O_5	SnO_2	Sb_2O_5	PbO	Total
P–T-417-R	Dull red	Mean	16.78	1.91	3.06	59.67	0.60	0.26	1.19	1.01	8.39	0.26	0.56	1.68	0.04	1.63	0.00	0.26	0.48	4.16	101.95
		SD	0.21	0.04	0.07	0.16	0.04	0.03	0.04	0.00	0.07	0.02	0.04	0.05	0.05	0.32	0.00	0.02	0.04	0.15	
S-423a-R	Dull red	Mean	13.85	2.67	1.90	53.88	0.23	0.96	0.89	1.76	7.74	0.14	0.27	1.11	0.01	1.33	0.02	0.49	0.22	10.92	98.46
		SD	0.13	0.05	0.06	0.57	0.04	0.01	0.05	0.02	0.01	0.01	0.04	0.07	0.04	0.08	0.02	0.04	0.06	0.27	
S-ARG-403-G	Yellow	Mean	11.82	0.53	2.12	69.85	0.05	0.30	1.19	0.49	5.80	0.08	0.14	1.24	0.01	0.05	0.01	0.01	0.92	5.34	99.94
		SD	0.36	0.02	0.02	1.71	0.01	0.01	0.09	0.01	0.32	0.03	0.03	0.18	0.01	0.04	0.01	0.02	0.06	1.86	
S-ArG-506-Ar	Yellowish-orange	Mean	10.97	1.39	1.99	40.47	0.52	0.32	1.10	0.91	5.22	0.23	0.16	1.65	0.01	7.93	0.03	0.91	0.38	27.73	101.92
		SD	0.11	0.03	0.04	0.31	0.05	0.08	0.07	0.02	0.03	0.02	0.05	0.03	0.01	0.68	0.03	0.08	0.06	0.24	
S-ArG-506-G	Yellowish-orange	Mean	11.12	1.81	1.97	40.93	0.76	0.40	0.76	1.08	5.53	0.19	0.42	1.52	0.01	9.25	0.03	1.24	0.57	22.69	100.26
		SD	0.20	0.05	0.01	0.24	0.05	0.03	0.08	0.01	0.03	0.04	0.05	0.06	0.01	0.18	0.03	0.02	0.23	0.66	
S-BiBR-404-R	Dull red	Mean	14.74	2.37	2.33	56.72	0.82	0.21	0.97	1.61	8.37	0.19	0.39	1.45	0.01	2.22	0.00	0.41	0.33	7.92	101.06
		SD	0.07	0.06	0.05	0.34	0.01	0.04	0.04	0.02	0.11	0.03	0.02	0.06	0.01	0.13	0.00	0.03	0.04	0.21	
S-BiBR-507-R	Dull red	Mean	14.11	2.83	2.08	54.15	1.10	0.18	1.06	1.70	7.88	0.19	0.42	1.57	0.02	1.62	0.00	0.46	0.25	9.90	99.49
		SD	0.22	0.06	0.06	0.28	0.03	0.03	0.02	0.02	0.02	0.01	0.07	0.04	0.02	0.05	0.00	0.03	0.03	0.17	
S-BiR-507-R	Dull red	Mean	13.79	2.62	2.38	57.20	1.14	0.23	1.00	2.07	8.18	0.18	0.46	1.42	0.01	1.71	0.01	0.40	0.39	8.34	101.53
		SD	0.15	0.10	0.04	0.21	0.06	0.04	0.03	0.06	0.05	0.02	0.02	0.07	0.02	0.12	0.02	0.02	0.05	0.35	
S-GA-005-Ar	Yellowish-orange	Mean	11.76	1.80	2.07	41.94	0.70	0.26	0.77	1.10	5.39	0.16	0.44	1.52	0.01	9.14	0.01	1.23	0.37	22.29	100.95
		SD	0.24	0.02	0.02	0.31	0.03	0.03	0.05	0.02	0.09	0.03	0.02	0.05	0.02	0.31	0.02	0.03	0.05	0.48	
S-GA-005-ArC	Yellowish-orange	Mean	11.31	1.39	2.10	41.00	0.49	0.25	1.18	0.90	5.25	0.22	0.16	1.68	0.03	7.02	0.02	0.93	0.38	27.72	102.02
		SD	0.20	0.07	0.05	0.35	0.05	0.02	0.04	0.01	0.07	0.03	0.02	0.07	0.04	0.53	0.02	0.01	0.04	0.36	
S-GA-005-ArS	Yellowish-orange	Mean	12.67	2.06	2.93	45.15	0.66	0.22	0.78	0.84	7.93	0.29	0.68	1.85	0.03	8.11	0.05	0.80	0.17	17.29	102.49
		SD	0.11	0.06	0.04	0.24	0.00	0.01	0.06	0.02	0.04	0.04	0.04	0.04	0.04	0.27	0.04	0.04	0.05	0.40	
S-GA-411-G	Yellow	Mean	13.96	0.52	2.06	66.28	0.05	0.27	1.15	0.55	5.77	0.14	0.11	1.15	0.01	0.01	0.02	0.00	0.90	7.84	100.81
		SD	0.18	0.03	0.07	1.08	0.01	0.04	0.03	0.03	0.22	0.01	0.03	0.31	0.02	0.01	0.01	0.00	0.02	0.96	

(Continues)

14754754, 2024, 1, Downloaded from https://onlinelibrary.wiley.com/doi/10.1111/arcm.12906 by CochraneItalia, Wiley Online Library on [04/02/2025]. See the Terms and Conditions (https://onlinelibrary.wiley.com/terms-and-conditions) on Wiley Online Library for rules of use; OA articles are governed by the applicable Creative Commons License

TABLE 1 (Continued)

Sample name	Glass color		Na_2O	MgO	Al_2O_3	SiO_2	SO_3	P_2O_5	Cl	K_2O	CaO	TiO_2	MnO	FeO	CoO	CuO	As_2O_5	SnO_2	Sb_2O_5	PbO	Total
S-GB-413-Ar	Yellowish-orange	Mean	11.83	1.64	2.95	44.98	0.66	0.32	0.71	1.07	7.06	0.21	0.26	2.40	0.01	6.86	0.06	0.92	0.42	18.18	100.54
		SD	0.33	0.04	0.06	0.30	0.06	0.04	0.03	0.03	0.06	0.03	0.03	0.12	0.01	0.66	0.01	0.03	0.03	0.50	
S-GR-506-Ar	Yellowish-orange	Mean	11.40	1.62	2.84	44.77	0.67	0.32	0.72	1.05	6.84	0.22	0.28	2.44	0.03	8.61	0.01	0.93	0.42	17.48	100.65
		SD	0.12	0.01	0.04	0.24	0.08	0.07	0.05	0.00	0.04	0.07	0.03	0.06	0.03	0.96	0.02	0.06	0.05	0.38	
S-GR-506-R	Sealing-wax red	Mean	10.35	0.97	1.74	39.00	0.41	0.34	0.78	0.92	4.63	0.15	0.17	1.20	0.00	4.83	0.04	0.88	0.52	32.68	99.63
		SD	0.17	0.05	0.05	0.39	0.03	0.07	0.02	0.01	0.03	0.01	0.01	0.09	0.01	0.17	0.03	0.01	0.04	0.07	
S-GRT-501-G	Yellowish-orange	Mean	11.48	1.74	2.01	42.63	0.75	0.38	0.77	1.10	5.47	0.20	0.41	1.41	0.03	8.04	0.01	1.25	0.39	21.67	99.75
		SD	0.30	0.04	0.04	0.97	0.05	0.07	0.04	0.03	0.14	0.04	0.03	0.02	0.04	1.02	0.02	0.05	0.15	0.19	
S-GRT-501-R	Dull red	Mean	13.84	2.56	2.28	56.28	1.15	0.26	0.99	2.07	8.05	0.18	0.43	1.37	0.01	1.72	0.01	0.39	0.34	7.87	99.81
		SD	0.32	0.07	0.08	0.26	0.05	0.04	0.02	0.02	0.09	0.03	0.02	0.05	0.01	0.31	0.03	0.05	0.03	0.27	
S-MR-502-M	Brown	Mean	10.51	0.36	1.55	57.25	0.11	0.30	0.53	0.46	0.73	0.15	0.75	1.61	0.01	7.63	0.15	0.22	1.12	17.68	101.11
		SD	0.26	0.04	0.04	0.90	0.05	0.07	0.04	0.03	0.13	0.03	0.03	0.02	0.02	0.50	0.02	0.05	0.15	0.19	
S-MR-502-R	Sealing-wax red	Mean	11.98	0.28	1.01	56.31	0.04	0.41	0.66	0.42	2.07	0.12	0.74	0.79	0.04	7.53	0.05	0.00	0.81	17.24	100.50
		SD	0.13	0.01	0.03	0.41	0.01	0.02	0.03	0.03	0.13	0.03	0.02	0.07	0.02	0.10	0.03	0.03	0.05	0.70	
S-RV-418-R1	Sealing-wax red	Mean	9.97	0.78	2.76	41.52	0.07	0.17	0.53	0.42	1.48	0.48	0.22	1.59	0.04	3.64	0.03	0.01	0.01	36.20	99.92
		SD	0.11	0.04	0.07	0.52	0.03	0.04	0.03	0.01	0.03	0.06	0.01	0.03	0.06	0.12	0.02	0.01	0.02	0.60	
S-RV-418-R2	Sealing-wax red	Mean	9.04	0.72	2.83	39.36	0.07	0.18	0.38	0.42	1.36	0.50	0.19	1.60	0.01	3.21	0.05	0.02	0.02	40.11	100.04
		SD	0.15	0.05	0.03	0.49	0.03	0.05	0.02	0.02	0.03	0.05	0.04	0.05	0.01	0.28	0.06	0.03	0.02	0.71	
S-RV-418-R2s	Sealing-wax red	Mean	8.92	0.82	3.22	45.07	0.11	0.23	0.43	0.55	1.28	0.57	0.21	1.82	0.02	3.56	0.03	0.00	0.00	34.50	101.34
		SD	0.32	0.03	0.04	0.26	0.04	0.04	0.02	0.02	0.05	0.06	0.06	0.14	0.03	0.65	0.03	0.00	0.01	0.32	
S-TR-501-R	Dull red	Mean	13.86	2.30	2.37	56.97	0.84	0.23	0.96	1.58	8.40	0.15	0.35	1.31	0.02	2.45	0.01	0.42	0.36	8.06	100.63
		SD	0.11	0.03	0.03	0.16	0.01	0.04	0.05	0.04	0.02	0.02	0.04	0.01	0.02	0.02	0.01	0.06	0.02	0.31	

14754754, 2024, 1, Downloaded from https://onlinelibrary.wiley.com/doi/10.1111/arcm.12906 by CochraneItalia, Wiley Online Library on [04/02/2025]. See the Terms and Conditions (https://onlinelibrary.wiley.com/terms-and-conditions) on Wiley Online Library for rules of use; OA articles are governed by the applicable Creative Commons License

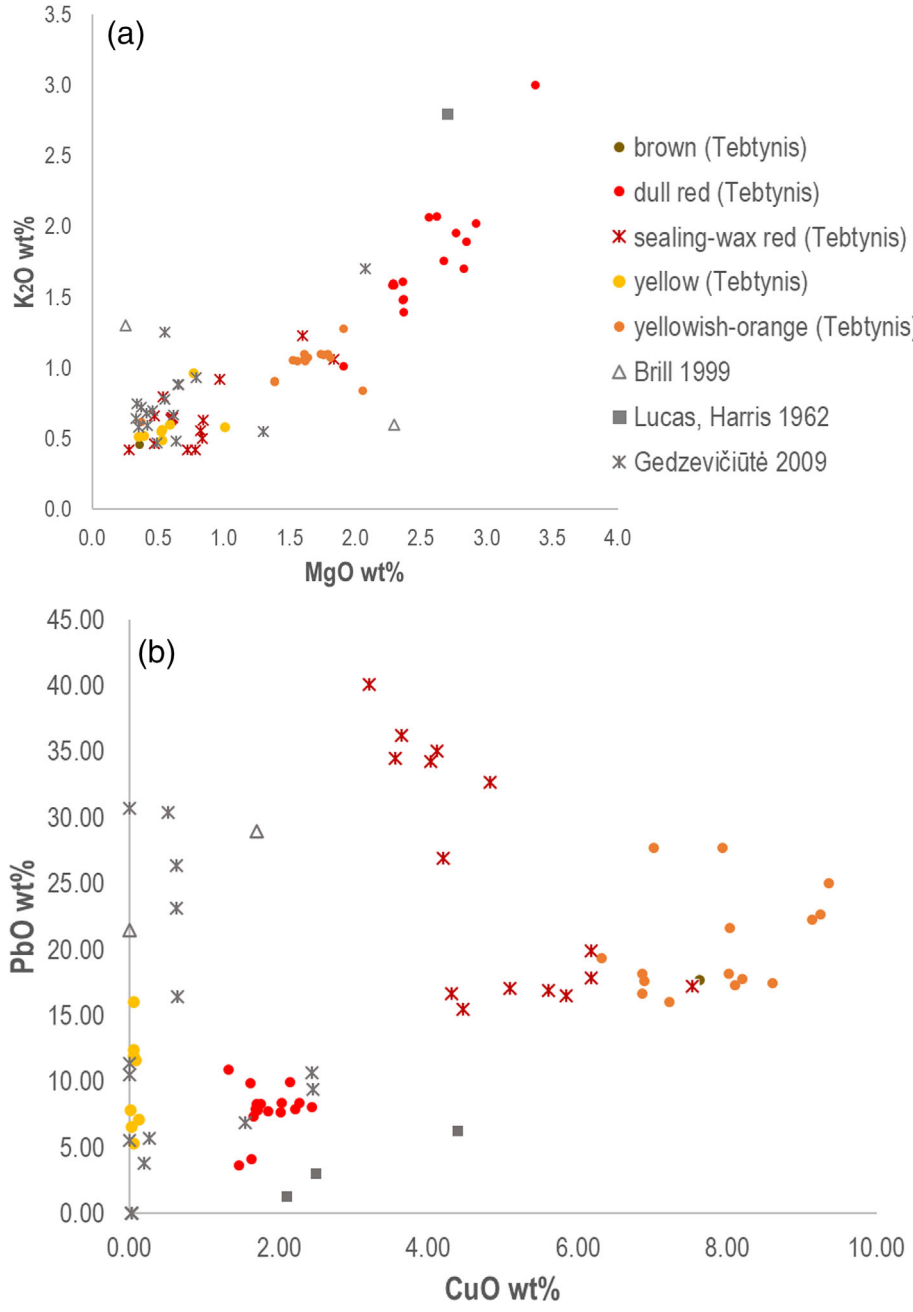

FIGURE 1 (a) K_2O versus MgO in the base glass of the glasses from Tebtynis (the color of the symbols corresponds to the color observed from macroscopic examination). (b) PbO versus CuO content in the base glass of the brown, yellow, dull red, and sealing-wax red glasses from Tebtynis (symbol: colored dots) compared to the coeval samples from Egypt analyzed by Brill (1999) (symbol: gray triangles), Lucas and Harris (1962) (symbol: gray squares), and Gedzevičiute et al. (2009) (symbol: gray asterisks).

between 48.56% and 54.60%, Sb_2O_5 between 31.30% and 33.87% and FeO between 4.34% and 4.83% (in P-FR-422-G1, P-A-402-G, and S-GA-411-G), and lead–tin antimonates (six occurrences) characterized by PbO ranging from 44.76% to 52.87%, Sb_2O_5 from 25.05% and 37.25%, SnO_2 from 1.71% to as high as 17.02%, and FeO from 1.16% to 4.44%.

14754754, 2024, 1, Downloaded from https://onlinelibrary.wiley.com/doi/10.1111/arcm.12906 by CochraneItalia, Wiley Online Library on [04/02/2025]. See the Terms and Conditions (https://onlinelibrary.wiley.com/terms-and-conditions) on Wiley Online Library for rules of use; OA articles are governed by the applicable Creative Commons License

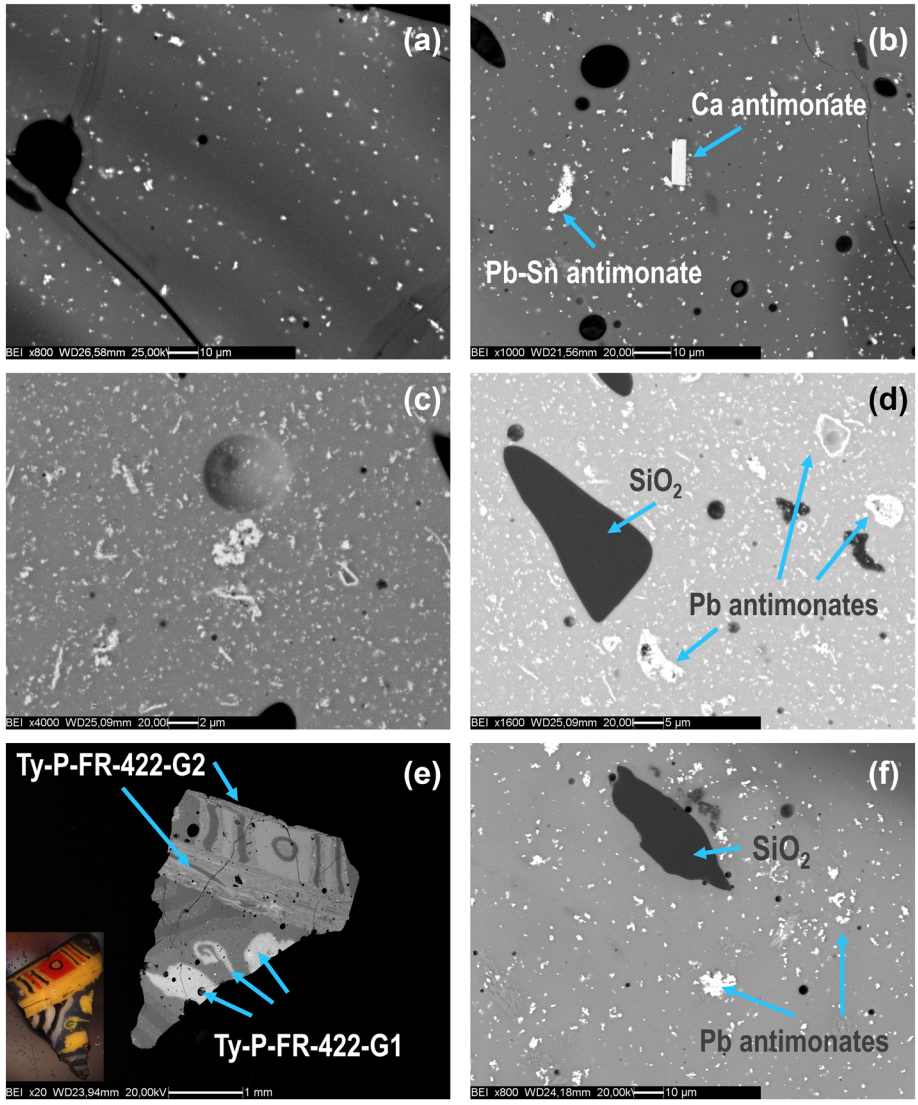

FIGURE 2 Texture and coloring/opacifying agents identified in opaque yellow glasses from Tebtynis: (a) Pb-banded texture in S-ARG-403-G; (b) calcium and lead–tin antimonates in P-FL-501-G; (c,d) uniform texture with evenly dispersed lead antimonates and quartz inclusions in P-A-402-G; (e) optical microscopical and backscattered electron images of P-FR-422, with two different types of opaque yellow glass—one with homogeneous texture (details of the flower, petals, and pistil) and the other with Pb-banded texture (simple bars); (f) lead antimonates and quartz inclusion in P-FR-422-G1.

Dull red glasses

Considering the alkali content, this class is notably different from the others, being characterized by high MgO (1.10–3.00%), K_2O (1.91–3.38%), CaO (7.42–9.13%), P_2O_5 (generally 0.16–0.34%, with two outliers at 0.76% and 0.96%, respectively), and SO_3 content (from 0.23% to peaks of 1.60% and an average of 0.99%), suggesting a plant-ash recipe for the base glass (Figure 1a). Dull reds exhibit intermediate levels of both CuO and PbO: respectively, 1.33%–2.45% and 1.92%–3.67% (Figure 1b).

14754754, 2024, 1, Downloaded from https://onlinelibrary.wiley.com/doi/10.1111/arcm.12906 by CochraneItalia, Wiley Online Library on [04/02/2025]. See the Terms and Conditions (https://onlinelibrary.wiley.com/terms-and-conditions) on Wiley Online Library for rules of use; OA articles are governed by the applicable Creative Commons License

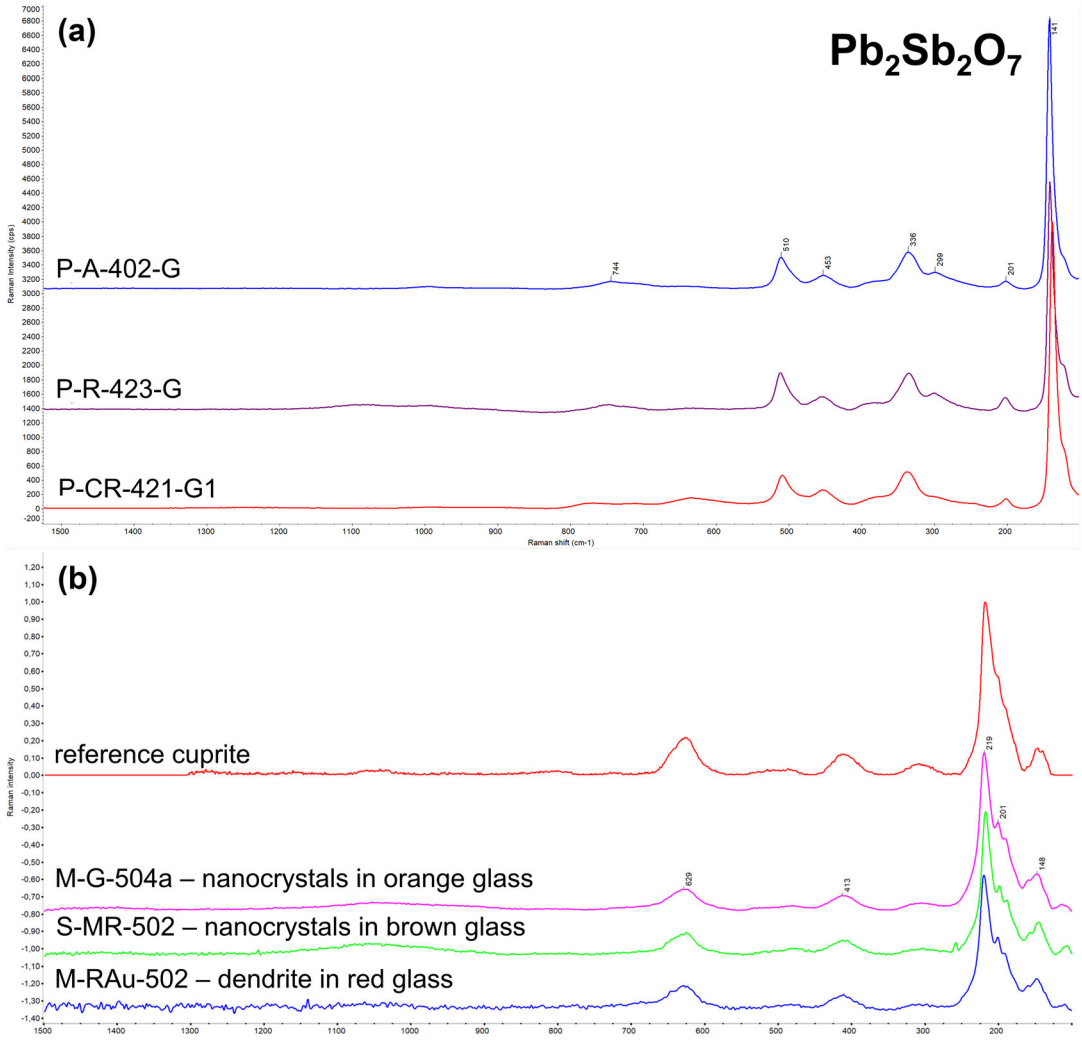

FIGURE 3 Raman spectra of (a) lead antimonates in the yellow samples P-A-402-G, P-R-423-G, and P-CR-421-G1; (b) cuprite dendrites and nanocrystals with cuprite reference spectrum (RRUFF web database, red line) in the yellowish-orange sample M-G-504a, in the brown sample S-MR-502-M, and in the sealing-wax red sample M-RAu-502.

Looking at OM and SEM-BSE images (Figure 4a), dull red glasses show a diffuse presence of nano-sized particles homogeneously dispersed in the vitreous phase. Despite their very limited size, which prevents a specific chemical characterization by EDS or WDS, they were interpreted as metallic copper considering textural features and micro-Raman analyses. Instead, the largest spheroidal inclusions (~1–5 μm) present in most samples were recognized as copper sulfides, especially chalcocite (Cu_2S), such as in P-A-418-R1 (WDS data: Cu 78.37% and S 18.47%).

Coming to the newly formed mineral phases, euhedral crystals of wollastonite are by far the most common occurrence, as they appear in most of the dull red glasses, often in large aggregates ranging from 5 to 100 μm. Sample P-FR-422-R also shows large aggregates of Ca-Pb-Na silicates that can be once more interpreted as devitrification products.

14754754, 2024, 1, Downloaded from https://onlinelibrary.wiley.com/doi/10.1111/arcm.12906 by CochraneItalia, Wiley Online Library on [04/02/2025]. See the Terms and Conditions (https://onlinelibrary.wiley.com/terms-and-conditions) on Wiley Online Library for rules of use; OA articles are governed by the applicable Creative Commons License

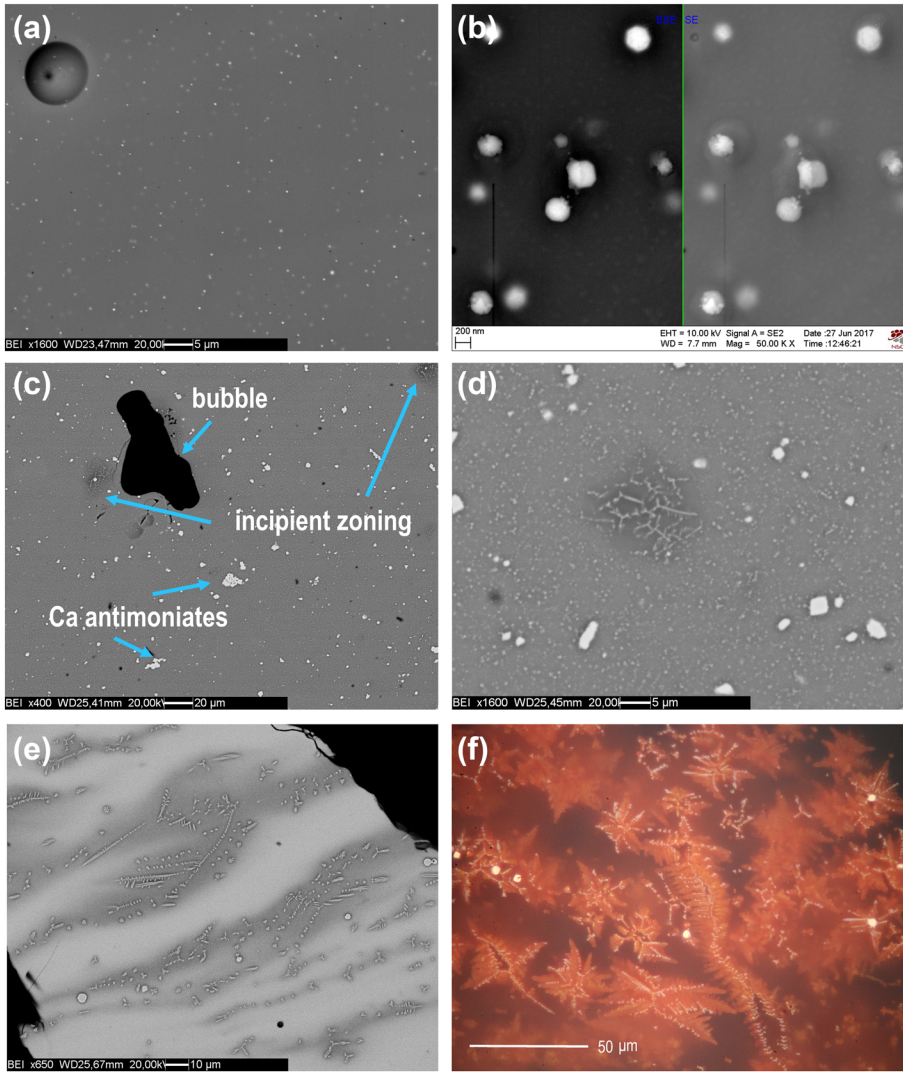

FIGURE 4 Scanning electron microscopical–backscattered electron and optical microscopical images of the texture and inclusions identified in the glasses from Tebtynis: (a) S-mix-006-R with nanometric metallic copper drops; (b) nanometric cuprite crystals in sample S-GB-413-Ar; (c,d) general view and detail of M-Ar-506 showing euhedral calcium–lead antimonates associated with nano-sized cuprite and areas with incipient dendritic crystal growth; (e) S-RV-418-R2 with banded texture, cuprite dendrites, and a series of metallic copper drops; (f) multifocal optical microscopical image (in shifted nicols) of metallic copper and cuprite crystals in S-RV-418-R1.

Residual batch minerals are rather scarce: one pyroxene with stoichiometry close to esseneit ($CaFe^{3+}AlSiO_6$), but lower in FeO, was found in P-FR-422-R (EDS data: $Al_2O_3 = 25.5\%$, $SiO_2 = 39.5\%$, $CaO = 24.0\%$, $FeO = 11.0\%$), while one alkali felspar with a mix of albite (EDS data: $Na_2O = 9.8\%$, $Al_2O_3 = 19.5\%$, $SiO_2 = 70.6\%$) and K-Na feldspar (EDS data: $Na_2O = 3.8\%$, $Al_2O_3 = 17.9\%$, $SiO_2 = 65.3\%$, $K_2O = 13.0\%$) was identified in sample P-CR-421-R.

14754754, 2024, 1, Downloaded from https://onlinelibrary.wiley.com/doi/10.1111/arcm.12906 by CochraneItalia, Wiley Online Library on [04/02/2025]. See the Terms and Conditions (https://onlinelibrary.wiley.com/terms-and-conditions) on Wiley Online Library for rules of use; OA articles are governed by the applicable Creative Commons License

Orange, sealing-wax red, and brown glasses

From the compositional point of view, yellowish-orange, brown, and sealing-wax red glasses form a continuous series, with a marked tendency toward higher PbO/CuO levels in red glasses.

Sealing-wax red and brown glasses were certainly produced starting from an LMG base glass, given the values of MgO (average 0.8%) and K_2O (average 0.67%) (Figure 1a). Sealing-wax red glasses show the highest PbO (15.50%–40.11%) and CuO (3.21%–7.53%) concentrations; however, the CuO versus PbO (Figure 1b) plot clearly indicates that they can be further divided into two subgroups on the basis of the PbO content: The first has PbO in the range of 15–20%, while the second has PbO varying from ~25% to 40%. Antimony also shows wide variations: one sample set has medium to high (0.40–1.61 wt%) and one very low Sb_2O_5 content (from below the detection limit to 0.02%).

Considering its overall chemical composition, the opaque brown glass S-MR-502-M stands in the lowest compositional range of sealing-wax reds, with PbO at 17.78% and CuO at 7.36%.

Conversely, the yellowish-orange samples exhibit an intermediate HMG-LMG composition, with low K_2O, in the range 0.71–1.28%, MgO between 1.56% and 2.06% and Na_2O from 13.59% to 17.19% (Figure 1a). They also have PbO from 16.06% to 27.73%, CuO between 6.31% and 9.36%, and low—but always present—antimony (0.17–0.57 wt%), except for sample M-Ar-506, with Sb_2O_5 at 1.90%.

The major colorant in the yellowish-orange, sealing-wax red, and brown series is cuprous oxide (Cu_2O) associated with a low number of metallic copper crystals (often with small copper sulfide segregations around the edges), as demonstrated by SEM-EDS and micro-Raman analyses (Figure 3b). From the textural point of view, yellowish-orange glasses are characterized by cuprite crystals of ~100–250 nm with octahedral habitus, as emerged from field emission gun (FEG)-SEM observations (Figure 4b). The brown glass S-MR-502-M has inclusions of a similar, nanometric size. Interestingly, euhedral crystals of calcium–lead antimonate are associated with nanoparticles of cuprite in M-Ar-506 (Figure 4c). This is consistent with the results of the chemical analyses, which highlighted higher Sb_2O_5 concentrations in this sample than for the typical yellowish-orange glasses from Tebtynis. M-Ar-506 is also unique for the presence of a few, small "pockets" depauperated in lead (darker in BSE), with incipient nucleation and growth of dendritic cuprite crystals (≤5 μm), attesting to an intermediate stage between classic yellowish-orange glasses and sealing-wax red glasses (Figure 4d).

Sealing-wax reds show two different types of texture: samples with PbO ≥ 30% approximately have well-defined bands of chemical zoning with stripes richer and poorer in lead (Figure 4e); low-lead areas contain most of the coloring agents, both cuprite dendrites (average size 1–60 μm) and metallic copper inclusions (average size 2–10 μm). It should be noted that SEM-BSE allows us to estimate the dimensions of the dendrite branches only in two dimensions, while the real extension of the inclusions can be studied qualitatively only by OM observations. In fact, crystals are dispersed in a transparent, greenish glass: by performing a series of stacked image acquisitions, it is possible to reconstruct the microstructure of the inclusions even inside the glassy matrix and obtain three-dimensional (3D) images of the crystals (Figure 4f).

Conversely, sealing-wax red samples with PbO comprised between 15% and 20% had very homogeneous vitreous phase, smaller cuprite dendrites (up to 20 μm), and a lower number of slightly larger metallic copper inclusions (5–15 μm). In general terms, there is a clear trend in the dimensions of the crystallites: in low-lead sealing-wax red glasses, they are smaller, with less-developed branching and cruciform or radial morphologies; conversely, in high-lead sealing-wax red glasses, they show complex dendritic shapes and exhibit a larger size, especially considering their tridimensional development as seen in OM observations. Samples with intermediate lead composition (25% ≤ PbO ≤ 30%) may sometimes exhibit evidence of zoning and incipient crystal growth.

14754754, 2024, 1, Downloaded from https://onlinelibrary.wiley.com/doi/10.1111/arcm.12906 by CochraneItalia, Wiley Online Library on [04/02/2025]. See the Terms and Conditions (https://onlinelibrary.wiley.com/terms-and-conditions) on Wiley Online Library for rules of use; OA articles are governed by the applicable Creative Commons License

Considering the newly formed phases in yellowish-orange glasses, wollastonite is the most frequent inclusion encountered, together with malayaite (i.e., $CaSnO(SiO_4)$), which was found in four out of 15 samples (S-ArG-506-Ar, S-GA-005-Ar, P-A-408-Ar, and S-GRT-501-Ar). Sand minerals are generally present within the bubbles or at the interface between glass layers of different colors and comprise quartz together with a wide number of Al, Fe and Fe–Ti oxides, and various types of feldspars and pyroxenes.

A similar situation appears in sealing-wax red glasses, which, however, do not show any tin-bearing crystalline inclusion. This is consistent with the lower levels of SnO_2 in the base glass, which has average values of 0.30% in sealing-wax red glasses and of 0.89% in yellowish-orange samples. Among the most peculiar crystals identified in the sealing-wax red class, the only occurrence of a lead copper halide mineral was identified with good confidence by WDS data as chloroxiphite (i.e., $Pb_3CuO_2Cl_2(OH)_2$). The crystal lies on the external surface of sample M-R-502d and most likely derives from the alteration of lead and copper-rich minerals in an evaporitic environment.

DISCUSSION

The glasses of the Tebtynis collection show a wide range of colors, varying from opaque yellow to red and brown, implying the use of different raw materials and a fully developed awareness of the pyro-technological processes related to the coloring and opacification of glass.

Principal component analysis (PCA; Figure 5) helps to summarize the main points: dull red glasses are characterized by significant concentrations of K_2O, MgO, CaO, and SO_3, showing the classic HMG recipe that is typical of plant ash glasses. All other samples have a natron-based composition, with elemental concentrations linked to the coloring process employed. The yellowish-orange samples show significant levels of FeO and Al_2O_3 and noteworthy levels of SnO_2; yellow glasses have the highest Sb_2O_5 and SiO_2 content in the dataset, associated with medium to low PbO. Sealing-wax red glasses can be divided into four subsets on the basis of the ratio PbO/Sb_2O_5 and PbO/CuO. Finally, the only opaque brown glass shares the main chemical trends of the sealing-wax red and yellowish-orange glasses.

From the textural and mineralogical point of view, these chemical differences correspond to the presence, size, and distribution of three different coloring and opacifying agents: (1) lead and lead–tin antimonates in yellow glasses; (2) nano-drops of metallic copper in dull red glasses; and (3) cuprite associated with micrometric particles of metallic copper in brown, yellowish-orange, and sealing-wax red glasses.

The color of the earliest yellow glasses found in Egypt and the Near East is invariably due to lead antimonates in the form of anhydrous, synthetic bindheimite with the formula $Pb_2Sb_2O_7$, sometimes labeled as Naples yellow (Mass et al., 1998; Shortland, 2008; Shortland & Eremin, 2006).

It has been reported that during the 4th century CE this traditional recipe is abandoned in favor of lead stannates (Lahlil et al., 2011; Tite et al., 2008). Verità et al. (2013), however, showed that the first examples of the use of tin-based yellow opacifiers can be traced back to the 2nd century CE in a series of *sectilia* panels discovered in the villa of the Roman emperor Lucius Verus.

Lahlil et al. (2011) and later Molina et al. (2014) demonstrated that lead antimonates found in yellow glasses from the New Kingdom can include traces of iron and zinc, while those found in Roman glasses (scattered *tesserae* with no stratigraphic references) generically dated from the 2nd century BCE and the 5th century CE usually contain small amounts of iron and moderate to high levels of tin. These data constitute an important chronological indicator for distinguishing the two productions. The lack of analyzed samples dated from the Late Period to the Early Ptolemaic era cannot clarify when (and where) this transition first took place in Egypt and the

14754754, 2024, 1, Downloaded from https://onlinelibrary.wiley.com/doi/10.1111/arcm.12906 by CochraneItalia, Wiley Online Library on [04/02/2025]. See the Terms and Conditions (https://onlinelibrary.wiley.com/terms-and-conditions) on Wiley Online Library for rules of use; OA articles are governed by the applicable Creative Commons License

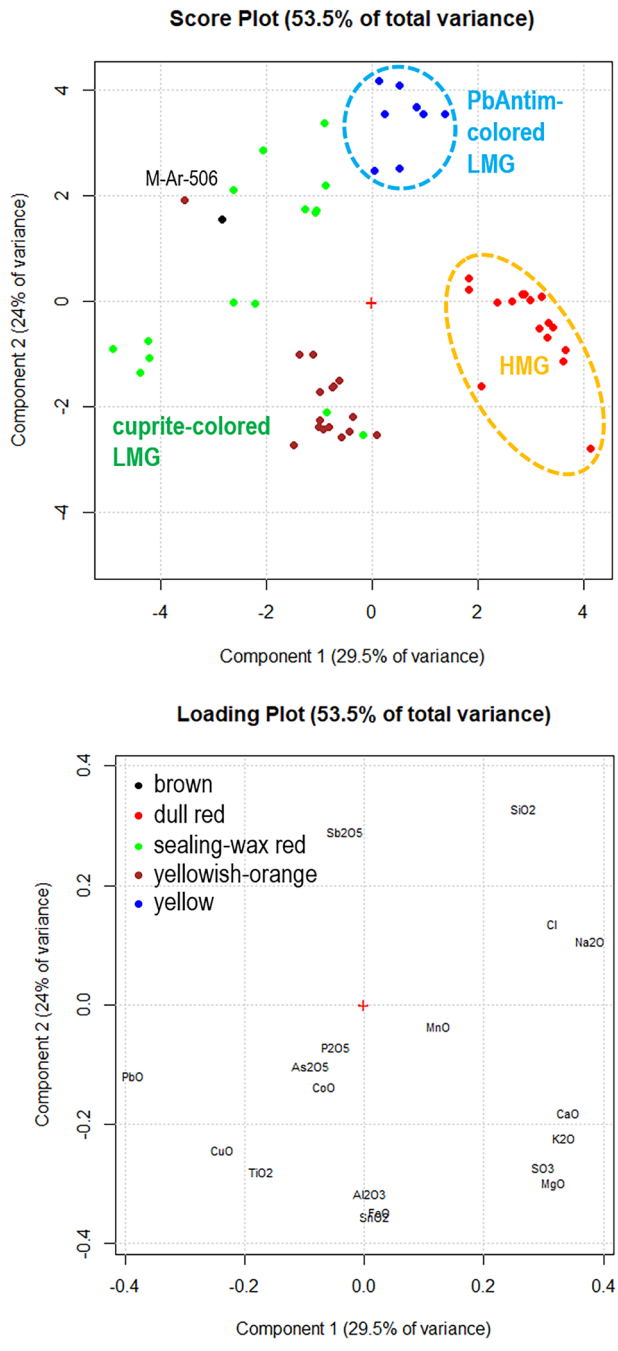

FIGURE 5 Principal component analysis score (up) and loading (down) plots of the yellow-orange-red and brown glasses from Tebtynis. Sample name is reported only for the outlier, while all other samples are classified according to their macroscopic color groups (symbols: black dot = brown glass; red dots = dull red glasses; green dots = sealing-wax red glass; orange dots = yellowish-orange glasses; blue dots = yellow glasses). LMG, low-magnesium glasses; HMG, high-magnesium glasses.

14754754, 2024, 1, Downloaded from https://onlinelibrary.wiley.com/doi/10.1111/arcm.12906 by CochraneItalia, Wiley Online Library on [04/02/2025]. See the Terms and Conditions (https://onlinelibrary.wiley.com/terms-and-conditions) on Wiley Online Library for rules of use; OA articles are governed by the applicable Creative Commons License

eventual correlations with the cultural, economic, and social context. The evidence provided by the beads discovered in Sardis suggests that in Anatolia this shift occurred at least as early as the 8th to 7th century BCE (Van Ham-Meert et al., 2019).

The analyses of a selection of antimonate inclusions in the yellow samples from Tebtynis show a significant correspondence with the Greco-Roman production, considering both the presence of iron (FeO ranging from 1.16% to 4.44%) and tin, even in very high amounts (1.71–6.13% with one crystal reaching 17.02 wt%), sufficient to account for lead–tin antimonates. These mixed lead–tin compounds are rather common in Roman glasses and were identified by numerous authors especially in mosaic *tesserae* and *sectilia* panels throughout the Imperial phase and during the Late Antiquity (see, e.g., Basso et al., 2014; Santagostino Barbone et al., 2008; Verità et al., 2013).

The data acquired during this work confirm that the transition zinc/tin in lead antimonate inclusions within ancient glasses occurs in Egypt at least from the late Ptolemaic period (~1st century BCE, but possibly even as early as the 3rd century BCE, according to the specific dating of the workshop, as discussed in Bettineschi, Deotto, et al., 2019), offering the chance to circumscribe the chronology for the introduction of this specific technique.

The Raman spectra of the antimonate inclusions in the Tebtynis samples are in good accordance with the results proposed by Rosi et al. (2009), showing that the deformation of the pyrochlore structure in the presence of tin causes the downfall of the peak at 510 cm^{-1}, which is the main band in unmodified lead antimonates, the appearance of a shoulder at ~450 cm^{-1}, and the shift of the band at 110 cm^{-1} to ~140 cm^{-1} (Figure 3a).

Interestingly, one yellow sample (P-FL-501-G) shows the combined presence of lead antimonates and calcium antimonates, where calcium antimonates are micrometric euhedral crystals in hexagonal form, compatible with an in situ crystallization. This evidence was never reported in ancient samples but was identified during experimental melts by Molina et al. (2014). These authors state that lead antimonate particles are stable in glass at temperatures from ~900 to 1000°C, before converting to calcium antimonate. Moreover, they suggest that the presence of tin and zinc improves the thermal stability of lead antimonate up to ~1100°C (Dik et al., 2005). However, the lead antimonates in P-FL-501-G have the highest SnO_2 content encountered in all the analyzed inclusions in the Tebtynis yellow glasses, reaching a significant value of 17.02%. This implies that temperatures higher than 1100°C must have been occasionally surpassed in the production of this specific sample, causing the partial fading of the yellow color while maintaining the opacification effect.

Considering the ratio PbO/Sb_2O_5, the yellow samples from Tebtynis exhibit values between 5.8 and 18.7, which are much higher than the stoichiometric ratio of the classic Naples yellow pigment (1.4). This means that yellow glasses were generally produced in excess of lead, an expedient possibly aimed at lowering the melting temperature and the viscosity of the glass and thus favoring stirring and avoiding color fading caused by thermal instability of the lead antimonates (Shortland, 2008). Additionally, lead is quite difficult to distribute throughout the glass because it tends to segregate, which might be one of the causes for the color zoning. The only exception is again sample P-FL-501-G, whose ratio is closer to that of the pigment, being 1.72. However, this effect may also be due to the conversion from lead to calcium antimonate, as noted above.

The idea of an ex situ synthesis of the lead/lead–tin antimonates or the *anime* compound (a synthetic lead antimony silicate) has been widely accepted among all authors both for Late Bronze Age (LBA) and Roman glass production. Freestone and Stapleton (2015) reported that the reduced composition of Roman yellow glasses usually shows higher silica content with respect to that of the other color classes. This evidence has been intended as a clue of the use of *anime* as coloring and opacifying agent, in contrast to the addition of lead antimonates. Looking at the reduced CaO versus SiO_2 concentrations (Supporting Information Table S3), it appears that yellow samples from Tebtynis do not show higher levels of silica with respect to

14754754, 2024, 1, Downloaded from https://onlinelibrary.wiley.com/doi/10.1111/arcm.12906 by CochraneItalia, Wiley Online Library on [04/02/2025]. See the Terms and Conditions (https://onlinelibrary.wiley.com/terms-and-conditions) on Wiley Online Library for rules of use; OA articles are governed by the applicable Creative Commons License

the reduced composition of other colors of the same collection. However, the tendency toward higher SiO_2 content in the loading plot of the PCA (Figure 5) may point in the same direction, for the majority of the samples.

From the textural point of view, antimonate-colored yellow glasses from Tebtynis can be distinguished in two main categories: five samples show peculiar lines of chemical zoning, defined by varying concentrations of PbO (as seen in, e.g., Mass et al., 2002; Shortland, 2008), while three samples have a very homogeneous texture with uniform distribution of the lead antimonate and lead–tin antimonates (also identified by Verità et al., 2013). It has been observed that zoned yellow glasses, especially common in LBA productions, can be associated with a higher viscosity of the glass melt, which complicates the even mixing of the pigment (Molina et al., 2014).

Moreover, sample P-A-402-G is characterized by the presence of numerous large, rounded quartz particles. Given their number, shape, size, and distribution pattern, they must be considered as an intentional addition, probably intended to improve the opacity as seen in other opaque blue or white glasses of different periods (e.g., Angelini et al., 2019; Maltoni & Silvestri, 2018). From what is published to date, this is the first documented occurrence of such a texture in yellow glasses that can perhaps be interpreted as one of the technical solutions tested by the Ptolemaic glassworkers that has never made it into the industrial-scale production of the Roman period.

Red glasses have always attracted much attention from researchers, as they testify to the mastery achieved by the ancient glassworkers in the control of the raw materials and of the firing conditions (Ahmed & Ashour, 1981; Angelini et al., 2004; Bandiera et al., 2019; Barber et al., 2010; Bimson, 1987; Brill & Cahill, 1988; Brun et al., 1991; Cable & Smedley, 1987; Drünert et al., 2018; Fiori, 2015; Freestone, 1987; Santagostino Barbone et al., 2008; Silvestri et al., 2014; Welham et al., 2000; Weyl, 1959). Red glass was also highly valued in antiquity and is one of the main subjects of the most ancient surviving glass recipes (Oppenheim et al., 1970).

Nowadays, all authors agree that copper, in different redox conditions, is responsible for the red color in most ancient glasses (except for gold ruby glasses); however, until the conclusive evidence presented by transmission electron microscopical analysis (Brun et al., 1991), considerable efforts were made to understand whether metallic copper (Cu^0) or cuprous oxide (synthetic cuprite, Cu_2O) nanoparticles was used as the main coloring/opacifying agent. It is now clear that the two forms were contemporary in use during the Roman period, and even in earlier times.

The first example of cuprite-colored glasses can be traced back to the New Kingdom Egypt: this technology was especially common at the site of Qantir/Pi-Ramesse, as demonstrated by Push and Rehren (2007). The typical sealing-wax red is due to the intrinsic color of the cuprite crystals, which are dispersed in a transparent, greenish glassy matrix.

Nanocrystals of metallic copper were, instead, found in the glasses produced in the Final Bronze Age site of Frattesina, in northern Italy, home of the so-called low-magnesium high-potassium (LMHK) mixed alkali glasses (Angelini et al., 2004). Nano-sized colloids of Cu^0 were also found in a glass rod from Amarna, Egypt, suggesting that both technologies were already in use during the New Kingdom (Barber et al., 2010). In this case, the dull red color can be attributed to the excitation of plasmon surface modes of copper nanoparticles, just like in the luster decorations known from Medieval times (Borgia et al., 2002).

The earliest cuprite-colored glasses can be distinguished from later productions as they usually contained very low or negligible amounts of lead. It is only in 9th-century BCE Iran that the role of lead in improving the formation of the red color is understood (Brill & Cahill, 1988). As noted by Freestone (1987), there are four main advantages of introducing lead into red glasses: (1) increasing the cuprite precipitation rate; (2) reducing the melting temperature; (3) reducing devitrification; (4) increasing the refractive index and thus the brilliance of the glass. This

14754754, 2024, 1, Downloaded from https://onlinelibrary.wiley.com/doi/10.1111/arcm.12906 by CochraneItalia, Wiley Online Library on [04/02/2025]. See the Terms and Conditions (https://onlinelibrary.wiley.com/terms-and-conditions) on Wiley Online Library for rules of use; OA articles are governed by the applicable Creative Commons License

technology is thought to have arrived in Egypt during the 7th to 6th century BCE (Bimson, 1987); it is certainly not the case that the first yellowish-orange inlays appear in Egypt in the *naos* of Darius I (British Museum, inv. EA37496), dated between the end of the 6th to early 5th century BCE.

Cuprite-colored orange and yellowish-orange glasses have been generally treated as a subset of cuprite-colored red glasses. As a matter of fact, they were probably first synthetized as an accidental by-product of sealing-wax red glasses, but—at least in the Tebtynis samples—they show significant compositional differences with respect to red samples in terms of proportions of the main constituents, quantity of minor and trace elements, and number of undissolved sand relics, which are significantly higher with respect to the sealing-wax red glasses and all other color classes. Ahmed and Ashour (1981) demonstrated that the color of the yellowish-orange glasses derives from the dispersion of cubic/octahedral cuprite crystals of colloidal size. This is consistent with the micro-Raman results (Figure 3b) on the Tebtynis glasses and with FEG-SEM observations (Figure 4b), which highlighted the presence of octahedral crystals of cuprite with size of the order of 100–250 nm.

Among the yellowish-orange glasses, M-Ar-506 shows both nano-sized cuprite and calcium–lead antimonates (WDS data) dispersed in the glassy matrix, associated with small pockets depauperated in lead, characterized by the incipient growth of dendritic cuprite crystals. Calcium antimonates were also noted in a sealing-wax red glass from Toprak Kale by Freestone (1987), who interpreted them as relics from the batch material. However, in the Tebtynis sample, this seems not the case. Calcium–lead antimonates are euhedral, thus suggesting a direct precipitation from the melt, possibly caused by an excess of antimony, which was found in an abundant set of the analyzed sealing-wax red glasses, as will be discussed later. Small pockets with preferential dendritic growth were also observed by Ahmed and Ashour (1981) during their experimental tests and were associated with temperatures of the order of 1000°C. These data constitute an important technological indicator, as they offer new hints on the production of the yellowish-orange and sealing-wax red glasses and on the delicate equilibrium necessary for producing the desired colors.

Contrary to what was proposed by Nenna and Gratuze (2009), this work proved that not all red glasses from Tebtynis have a plant ash composition. Indeed, the HMG recipe is restricted to the Cu^0-colored dull red glasses, while all the cuprite-colored red samples we analyzed range in the variability of LMG glasses. However, it should be noted that the technology and raw materials of MgO- and K_2O-rich red glasses have been widely discussed over the years, with certain authors suggesting that they were produced by adding fuel ashes to an existing natron glass (Fiori, 2015; Freestone & Stapleton, 2015; Maltoni & Silvestri, 2018) and others arguing them to be plant ash glasses, independent from the natron production (Bandiera et al., 2020; Paynter et al., 2015). Judging from the Tebtynis assemblage, which demonstrate that colorless HMG glasses were also in circulation at the time (Bettineschi & Angelini, 2022), we are more inclined to sustain this second option.

As already noted, yellowish-orange samples also have higher K_2O and MgO contents with respect to the classic LMG recipe (threshold values of 1.5% for both alkali, according to Lilyquist & Brill, 1993); however, this difference seems due rather to the use of very impure sands rich in K- and Mg-bearing minerals (as also observed by SEM-EDS) or most probably to an intentional or unintentional pollution by the fuel ashes and the charcoal during the coloring process, as previously proposed also for emerald green Roman glasses (Jackson & Cottam, 2015). This kind of contamination was surely observed in two sealing-wax red glasses from Tebtynis, while all other samples show the usual chemical signature of natron glasses, in terms of potash and magnesia.

Considering the main compositional classes of the copper-colored red (both dull red and sealing-wax red), brown, and yellowish-orange glasses proposed in the literature

14754754, 2024, 1, Downloaded from https://onlinelibrary.wiley.com/doi/10.1111/arcm.12906 by CochraneItalia, Wiley Online Library on [04/02/2025]. See the Terms and Conditions (https://onlinelibrary.wiley.com/terms-and-conditions) on Wiley Online Library for rules of use; OA articles are governed by the applicable Creative Commons License

(e.g., Fiori, 2015; Freestone et al., 2003; Silvestri et al., 2014), the samples from Tebtynis can be distinguished in the following groups based on the CuO and PbO contents:

1. low copper (CuO 1.46–2.45%), medium lead (PbO 3.67–10.92%), which is associated with metallic copper nanoparticles;
2. medium copper (CuO 3.21–4.83%), very high lead (PbO 32.68–40.11%), which is characteristic of cuprite-colored sealing-wax red glasses with zoned glassy matrix;
3. high copper (CuO 4.04–6.19%), high lead (PbO 15.50–19.93%), which is typical of cuprite-colored sealing-wax red glasses with no chemical zoning of the glassy matrix;
4. very high copper (CuO 6.31–9.36%), high lead (PbO 16.26–27.73%), which is typical of cuprite-colored yellowish-orange glasses, but includes one sealing-wax red and one brown sample.

The only exception is a sealing-wax red sample (I-RAu-605) showing an intermediate composition with medium CuO (4.19%) and high PbO (26.93%).

These groups are in good agreement with the textural characteristics of the samples and with compositional classes emerging from the PCA, which indicates a series of other significant differences, especially related to minor and trace elements.

Looking at the microstructure of the sealing-wax red glasses with medium CuO and very high PbO, they are characterized by bands of chemical zoning, with stripes richer (light gray in BSE) and poorer (dark gray in BSE) in lead. Inclusions of both dendritic cuprite and metallic copper are mostly concentrated in the darker areas. Conversely, high-CuO–high-PbO glasses have a uniform appearance, with uniformly dispersed dendrites.

It has been stated that the color of the cuprite crystallites is a function of their size, which, in turn, depends on the firing time/temperature, the type of heat treatment, and the composition of the base glass (Cable & Smedley, 1987; Welham et al., 2000). This pattern is confirmed by the Tebtynis samples: in fact, the yellowish-orange samples are associated with colloidal-size cuprous oxide particles. The progressive increase in the crystal size during heat treatment leads to the development of the red dendrites: the biggest Cu_2O crystals can be found in the zoned, medium CuO–very high PbO glasses, where they reach dimensions up to 70 μm.

Antimony is rather frequent in a set of sealing-wax red glasses, yellowish-orange, and brown glasses from Tebtyins (up to 1.90 wt%). Brill and Cahill (1988) have suggested that antimony might have been added as an internal reducing agent and/or as a decolorizer in order to decrease the greenish tint of the base glass and thus improve the overall color intensity and the brilliance of the final products. Freestone et al. (2003) pointed out that not all opaque cuprite red glasses show significant amounts of antimony and that the use of recycled glass may account for some of the analyzed occurrences. In the case of the Tebtynis glasses, the very high levels identified in at least some of the samples seem to speak in favor of an intentional, but non-systematic addition.

Tin is also frequently cited as an additive for facilitating the precipitation of cuprous oxide (Freestone et al., 2003; Shugar, 2000), so its frequency in the yellowish-orange glasses from Tebtynis is no surprise. The average values of Cu/Sn in this color class are 8–9 in weight, which is very close to the ratio of the classic bronze alloys produced in antiquity, thus suggesting that tin was added to the melt in the form of scrap bronze.

Yellowish-orange samples are also characterized by high FeO (up to 2.44%) and a considerable number of residual phases, especially hematite, as emerged from the micro-Raman investigations. Unfortunately, it is not possible to know if the FeO levels are only due to the use of a particularly impure sand or if iron was intentionally added as a reducing agent, as already proposed in other case studies from the literature (Maltoni & Silvestri, 2018; Silvestri et al., 2014).

Figure 1 shows that lead antimonate yellow glasses are relatively common in the published sample sets from Greco-Roman Egypt. However, the plot also highlights the lack of analyzed

14754754, 2024, 1, Downloaded from https://onlinelibrary.wiley.com/doi/10.1111/arcm.12906 by CochraneItalia, Wiley Online Library on [04/02/2025]. See the Terms and Conditions (https://onlinelibrary.wiley.com/terms-and-conditions) on Wiley Online Library for rules of use; OA articles are governed by the applicable Creative Commons License

yellowish-orange and sealing-wax red samples produced using cuprite as a coloring and opacifying agent, except for those from Tebtynis considered during this work. This is certainly due to the low number of published analytical studies related to this period and geographical area. As already noted, yellowish-orange glasses appeared in Egypt at least from the 6th century BCE and were already widespread by the second half of the 4th century BCE, as suggested by their abundant use in the sarcophagi of the brothers *Petosiris* and *Djedthotiuefankh* (Bettineschi, Angelini, & Molin, 2019). Thus, the lack of comparative data in that specific area of the plot should not be considered in terms of absence from the archaeological record, but only as a bias created by the selection of samples analyzed to date.

CONCLUSIONS

The chemical, mineralogical, and microstructural analysis of the Tebtynis samples provides the first systematic study on the coloring and opacifying technologies employed by the Ptolemaic artisans for producing yellow, yellowish-orange, red, and opaque brown glass.

As already observed in other color classes from the same site and chronology (Bettineschi & Angelini, 2022), our analyses clearly show the coexistence of glasses produced using two different alkali sources: while the classic LMG composition, typical of the Middle to Final Iron Age and of the Roman glass, is clearly predominant, a few samples are consistent with the use of plant ash as a flux (HMG). This recipe is especially typical (but not exclusive) of dull red glasses colored by metallic copper and can probably be associated with the strongly reducing conditions, which were needed for the manufacture of this specific color. Other intermediate compositions such as those of the yellowish-orange samples were interpreted in terms of natron-based glasses, which were subject to compositional changes occurring during the coloring process.

Lead can also decrease the melting point and thus act as a flux. In the investigated samples, PbO is present in different concentrations, from 5 up to 40 wt%, thus characterizing them as soda-lime–lead and leaded glasses.

At the same time, it was possible to identify peculiar samples that are apparently unique, at least according to our current understanding of first-millennium BCE Mediterranean glassmaking: this is the case of the lead antimonate yellow glass with intentional addition of abundant quartz grains, of the orange sample with pockets of incipient dendritic growth and a number of clacium antimonate, euhedral crystals, or of the yellow glass with both calcium and lead antimonates, and many others. It is thus clear that the Ptolemaic age is a time of innovation and experimentation, and while some solutions retained a significant success in the following periods, others were completely lost or discarded.

This work also contributes to offering a chronological staple for the introduction of specific coloring techniques, such as the cuprite-colored yellowish-orange glasses. It is also interesting to note that lead antimonate yellow glasses—which can be considered as heir of the LBA tradition—were found associated (at times even within the same inlay) with cuprite-based yellowish-orange glasses that represent a novelty of the mid-first millennium BCE and become increasingly common during the Roman and Byzantine periods.

There is still much to do before we reach a deeper understanding of Ptolemaic glass. Future investigations are expected to further expand our knowledge on the base glass production and provenance, the glass-forming, and glass-coloring techniques, the furnace conditions, and the raw materials used. Yet, this work clearly shows that a systematic, multi-methodological approach can offer substantial, novel insights and pave the way for fostering a robust framework aimed at interpreting the development of glass in this key moment of its history.

14754754, 2024, 1, Downloaded from https://onlinelibrary.wiley.com/doi/10.1111/arcm.12906 by CochraneItalia, Wiley Online Library on [04/02/2025]. See the Terms and Conditions (https://onlinelibrary.wiley.com/terms-and-conditions) on Wiley Online Library for rules of use; OA articles are governed by the applicable Creative Commons License

AUTHOR CONTRIBUTIONS

Conceptualization, methodology, sampling, validation, and data interpretation: Cinzia Bettineschi and Ivana Angelini. *Software, formal analysis, investigation, data curation, visualization, and writing—original draft preparation*: Cinzia Bettineschi. *Writing—review and editing*: Cinzia Bettineschi and Ivana Angelini. *Supervision*: Ivana Angelini. All authors have read and agreed to the published version of the manuscript.

ACKNOWLEDGEMENTS

The *Museo Egizio*, *Torino*, and the *Soprintendenza Archeologia*, *Belle Arti e Paesaggio per la città metropolitana di Torino*, particularly Christian Greco, Alessia Fassone, and Matilde Borla, are heartfully thanked for favoring access to the materials and for sampling authorizations. Gianmario Molin and Paola Zanovello are also sincerely acknowledged for their support of the project. The reviewers are thanked for contributing to improve the final draft of the paper.

DATA AVAILABILITY STATEMENT

The data that support the findings of this study are all included within this article and in its supplementary materials.

ORCID

Cinzia Bettineschi https://orcid.org/0000-0001-5322-4815
Ivana Angelini https://orcid.org/0000-0002-7970-3416

REFERENCES

Ahmed, A., & Ashour, G. M. (1981). Effect of heat treatment in the crystallisation of cuprous oxide in glass. *Glass Technology*, *22*, 24–33.

Angelini, I., Gratuze, B., & Artioli, G. (2019). Glass and other vitreous materials through history. In *The contribution of mineralogy to cultural heritage* (pp. 87–150). Mineralogical Society of Great Britain & Ireland. https://doi.org/10.1180/EMU-notes.20.3

Angelini, I., Artioli, G., Bellintani, P., Diella, V., Gemmi, M., Polla, A., & Rossi, A. (2004). Chemical analyses of bronze age glasses from Frattesina Di Rovigo, northern Italy. *Journal of Archaeological Science*, *31*(8), 1175–1184. https://doi.org/10.1016/j.jas.2004.02.015

Bandiera, M., Lehuédé, P., Verità, M., Alves, L., Biron, I., & Vilarigues, M. (2019). Nanotechnology in Roman opaque red glass from the 2nd century AD. Archaeometric investigation in red sectilia from the decoration of the Lucius Verus Villa in Rome. *Heritage*, *2*(3), 2597–2611. https://doi.org/10.3390/heritage2030159

Bandiera, M., Verità, M., Lehuédé, P., & Vilarigues, M. (2020). The technology of copper-based red glass sectilia from the 2nd century AD Lucius Verus villa in Rome. *Minerals*, *10*(10), 875. https://doi.org/10.3390/min10100875

Barber, D., Freestone, I., & Moulding, K. (2010). Ancient copper red glasses: Investigation and analysis by microbeam techniques. *From Mine to Microscope – Advances in the Study of Ancient Technology*, *37*(4), 898–899. https://doi.org/10.1016/j.jas.2009.11.021

Basso, E., Invernizzi, C., Malagodi, M., La Russa, M. F., Bersani, D., & Lottici, P. P. (2014). Characterization of colorants and opacifiers in Roman glass mosaic tesserae through spectroscopic and spectrometric techniques. *Journal of Raman Spectroscopy*, *45*(3), 238–245. https://doi.org/10.1002/jrs.4449

Bettineschi, C., & Angelini, I. (2022). Reflections into Ptolemaic glass: Colorless, white, blue, and green inlays from the workshop of Tebtynis. *Archaeometry*, *65*, 653–690. https://doi.org/10.1111/arcm.12825

Bettineschi, C., Angelini, I., & Molin, G. (2019). Contestualizzazione Degli Intarsi in Vetro Da Tebtynis Nel Quadro Dell'Egitto Greco-Romano. In I. Favaretto, F. Ghedini, P. Zanovello, & E. M. Ciampini (Eds.), *Anti. Archeologia. Archivi* (pp. 515–540). IVSLA Edizioni.

Bettineschi, C., Deotto, G., Begg, D. J. I., Molin, G., Zanovello, P., Fassone, A., Greco, C., Borla, M., & Angelini, I. (2019). A dig through archives and depots: Rediscovering the inlay workshop of Tebtynis and its materials. *Nuncius*, *34*(3), 485–516. https://doi.org/10.1163/18253911-03403001

Bimson, M., & Freestone, I. C. (1988). Some Egyptian glasses dated by royal inscriptions. *Journal of Glass Studies*, *30*, 11–15.

Bimson, M. (1987). Opaque red glass. A review of the previous studies. In *Early vitreous materials* (pp. 165–171). Brotish Museum.

14754754, 2024, 1, Downloaded from https://onlinelibrary.wiley.com/doi/10.1111/arcm.12906 by CochraneItalia, Wiley Online Library on [04/02/2025]. See the Terms and Conditions (https://onlinelibrary.wiley.com/terms-and-conditions) on Wiley Online Library for rules of use; OA articles are governed by the applicable Creative Commons License

Borgia, I., Brunetti, B., Mariani, I., Sgamellotti, A., Cariati, F., Fermo, P., Mellini, M., Viti, C., & Padeletti, G. (2002). Heterogeneous distribution of metal nanocrystals in glazes of historical pottery. *Applied Surface Science*, *185*(3–4), 206–216. https://doi.org/10.1016/S0169-4332(01)00659-6

Brill, R. H. (1999). *Chemical analysis of early glasses. Tables of analyses* (Vol. 2, p. 335). Corning Museum of Glass.

Brill, R. H., & Cahill, N. D. (1988). A red opaque glass from Sardis and some thoughts on red opaques in general. *Journal of Glass Studies*, *30*, 16–27.

Brun, N., Mazerolles, L., & Pernot, M. (1991). Microstructure of opaque red glass containing copper. *Journal of Materials Science Letters*, *10*(23), 1418–1420. https://doi.org/10.1007/BF00735696

Cable, M., & Smedley, J. W. (1987). The replication of an opaque red glass from Nimrud. In *Early vitreous materials* (pp. 151–164). British Museum.

Dik, J., Hermens, E., Peschar, R., & Schenk, H. (2005). Early production recipes for lead antimonate yellow in Italian art. *Archaeometry*, *47*(3), 593–607. https://doi.org/10.1111/j.1475-4754.2005.00221.x

Drünert, F., Palamara, E., Zacharias, N., Wondraczek, L., & Möncke, D. (2018). Ancient Roman nano-technology: Insight into the manufacture of mosaic tesserae opacified by calcium Antimonate. *Journal of the European Ceramic Society*, *38*(14), 4799–4805. https://doi.org/10.1016/j.jeurceramsoc.2018.06.031

Fiori, C. (2015). Production technology of Byzantine red mosaic glasses. *Ceramics International*, *41*(2), 3152–3157. https://doi.org/10.1016/j.ceramint.2014.10.160

Freestone, I. C. (1987). Composition and microstructure of early opaque red glass. In M. Bimson & I. C. Freestone (Eds.), *Early vitreous materials* (pp. 173–191). British Museum.

Freestone, I. C., & Stapleton, C. P. (2015). Composition, technology and production of coloured glasses from mosaic vessels of the early Roman empire. In J. Bayley, I. C. Freestone, & C. M. Jackson (Eds.), *Glass of the Roman empire* (pp. 61–76). Oxbow books.

Freestone, I. C., Stapleton, C. P., & Rigby, V. (2003). The production of red glass and enamel in the late iron age, Roman and Byzantine periods. In *Through a glass brightly: Studies in Byzantine and medieval art and archaeology* (pp. 142–154). Oxbow Books. https://doi.org/10.2307/j.ctvh1dktz.23

Gedzevičiute, V., Welter, N., Schüssler, U., & Weiss, C. (2009). Chemical composition and colouring agents of Roman mosaic and millefiori glass, studied by electron microprobe analysis and raman microspectroscopy. *Archaeological and Anthropological Sciences*, *1*(1), 15–29. https://doi.org/10.1007/s12520-009-0005-4

Grose, D. F. (1989). *Early ancient glass*. Hudson Hills Press.

Jackson, C. M., & Cottam, S. (2015). 'A green thought in a green shade'; compositional and typological observations concerning the production of emerald green glass vessels in the 1st century A.D. *Journal of Archaeological Science*, *61*, 139–148. https://doi.org/10.1016/j.jas.2015.05.004

Lahlil, S., Cotte, M., Biron, I., Szlachetko, J., Menguy, N., & Susini, J. (2011). Synthesizing lead antimonate in ancient and modern opaque glass. *Journal of Analytical Atomic Spectrometry*, *26*(5), 1040–1050. https://doi.org/10.1039/c0ja00251h

Lilyquist, C., & Brill, R. H. (1993). In C. Lilyquist & R. H. Brill (Eds.), *Studies in early Egyptian glass*. The Metropolitan Museum of Art.

Lucas, A., & Harris, J. R. (1962). *Ancient Egyptian materials and industries* (4th ed.). London: Edward Arnold Publishers.

Maltoni, S., & Silvestri, A. (2018). Innovation and tradition in the fourth century mosaic of the Casa Delle Bestie Ferite in Aquileia, Italy: Archaeometric characterisation of the glass tesserae. *Archaeological and Anthropological Sciences*, *10*(2), 415–429. https://doi.org/10.1007/s12520-016-0359-3

Mass, J. L., Stone, R. E., & Wypyski, M. T. (1998). The mineralogical and metallurgical origins of Roman opaque colored glasses. In P. McCray & W. D. Kingery (Eds.), *The prehistory and history of glassmaking technology* (pp. 251–268). The American Ceramics Society.

Mass, J. L., Wypyski, M. T., & Stone, R. E. (2002). Malkata and Lisht glassmaking technologies: Towards a specific link between second millennium BC metallurgists and glassmakers. *Archaeometry*, *44*(1), 67–82. https://doi.org/10.1111/1475-4754.00043

Molina, G., Odin, G. P., Pradell, T., Shortland, A. J., & Tite, M. S. (2014). Production technology and replication of lead antimonate yellow glass from New Kingdom Egypt and the Roman empire. *Journal of Archaeological Science*, *41*, 171–184. https://doi.org/10.1016/j.jas.2013.07.030

Nenna, M.-D., & Gratuze, B. (2009). Étude Diachronique Des Compositions de Verres Employés Dans Les Vases Mosaiqués Antiques: Résultats Préliminarires. In P. Koen Janssens, P. C. Degryse, J. Caen, & L. Van't dack (Eds.), *Annales Du 17e 'ongrès de l'Association Internat'onal Pour l'Histoire Du Verre, Anvers 2006* (pp. 199–205). University Press Antwerp. https://doi.org/10.13140/2.1.2923.7121

Oppenheim, A. L., Brill, R. H., von Saldern, A., & Barag, D. (Eds.). (1970). *Glass and glassmaking in ancient Mesopotamia*. Corning Museum of Glass.

Paynter, S., Kearns, T., Cool, H., & Chenery, S. (2015). Roman Coloured glass in the western provinces: The glass cakes and tesserae from west Clacton in England. *Journal of Archaeological Science*, *62*, 66–81. https://doi.org/10.1016/j.jas.2015.07.006

14754754, 2024, 1, Downloaded from https://onlinelibrary.wiley.com/doi/10.1111/arcm.12906 by CochraneItalia, Wiley Online Library on [04/02/2025]. See the Terms and Conditions (https://onlinelibrary.wiley.com/terms-and-conditions) on Wiley Online Library for rules of use; OA articles are governed by the applicable Creative Commons License

Push, E., & Rehren, T. (2007). Hochtemperatur-Technologie in Der Ramses-Stadt. In *Rubinglas Für Den Pharao*. Hildesheim.

Rosi, F., Manuali, V., Miliani, C., Brunetti, B. G., Sgamellotti, A., Grygar, T., & Hradil, D. (2009). Raman scattering features of lead pyroantimonate compounds. Part I: XRD and Raman characterization of Pb2Sb2O7 doped with tin and zinc. *Journal of Raman Spectroscopy*, *40*(1), 107–111. https://doi.org/10.1002/jrs.2092

Santagostino Barbone, A., Gliozzo, E., D'acapito, F., Memmi Turbanti, I., Turchiano, M., & Volpe, G. (2008). The sectilia panels of Faragola (Ascoli Satriano, southern Italy): A multi-analytical study of the red orange and yellow glass slabs. *Archaeometry*, *50*(3), 451–473. https://doi.org/10.1111/j.1475-4754.2007.00341.x

Shortland, A. J. (2008). The use and origin of antimonate colorants in early Egyptian glass*. *Archaeometry*, *44*(4), 517–530. https://doi.org/10.1111/1475-4754.t01-1-00083

Shortland, A. J., & Eremin, K. (2006). The analysis of second millennium glass from Egypt and Mesopotamia, part 1: New WDS analysis. *Archaeometry*, *48*(4), 581–603. https://doi.org/10.1111/j.1475-4754.2006.00274.x

Shugar, A. N. (2000). Byzantine opaque red glass tesserae from Beit Shean, Israel. *Archaeometry*, *42*(2), 375–384. https://doi.org/10.1111/j.1475-4754.2000.tb00888.x

Silvestri, A., Tonietto, S., Molin, G., & Guerriero, P. (2014). The Palaeo-Christian glass mosaic of St. Prosdocimus (Padova, Italy): Archaeometric characterisation of tesserae with copper- or tin-based opacifiers. *Journal of Archaeological Science*, *42*(1), 51–67. https://doi.org/10.1016/j.jas.2013.10.018

Stern, E. M. (2012). Glass production. In *The Oxford handbook of engineering and technology in the classical world* (pp. 1–30). Oxford Academic. https://doi.org/10.1093/oxfordhb/9780199734856.013.0022

Tite, M., Pradell, T., & Shortland, A. (2008). Discovery, production and use of tin-based opacifiers in glasses, enamels and glazes from the late iron age onwards: A reassessment. *Archaeometry*, *50*(1), 67–84. https://doi.org/10.1111/j.1475-4754.2007.00339.x

Van Ham-Meert, A., Dillis, S., Blomme, A., Cahill, N., Claeys, P., Elsen, J., Eremin, K., Gerdes, A., Steuwe, C., Roeffaers, M., & Shortland, A. (2019). A unique recipe for glass beads at iron age Sardis. *Journal of Archaeological Science*, *108*(June), 104974. https://doi.org/10.1016/j.jas.2019.104974

Verità, M., Maggetti, M., Saguì, L., & Santopadre, P. (2013). Colors of Roman glass: An investigation of yellow sectilia in the Gorga collection. *Journal of Glass Studies*, *55*, 39–52.

Welham, K., Jackson, C. M., & Smedley, J. W. (2000). Colour formation in sealing-wax red glass. In *Annales Du 14e Congrès de l'Association International Pour l'Histoire Du Verre, Amsterdam 1998* (pp. 11–15). AIHV.

Weyl, W. A. (1959). *Coloured glass*. Dawson.

SUPPORTING INFORMATION

Additional supporting information can be found online in the Supporting Information section at the end of this article.

How to cite this article: Bettineschi, C., & Angelini, I. (2024). Reflections into Ptolemaic Glass II: Characterizing Yellow, Yellowish-orange, Red, and Brown Inlays from Tebtynis. *Archaeometry*, *66*(1), 119–141. https://doi.org/10.1111/arcm.12906

14754754, 2024, 1, Downloaded from https://onlinelibrary.wiley.com/doi/10.1111/arcm.12906 by CochraneItalia, Wiley Online Library on [04/02/2025]. See the Terms and Conditions (https://onlinelibrary.wiley.com/terms-and-conditions) on Wiley Online Library for rules of use; OA articles are governed by the applicable Creative Commons License